https://doi.org/10.5194/egusphere-2026-1792
Preprint. Discussion started: 8 May 2026

Turbulent atmospheric particle fluxes in the high Arctic: Surface type dependence and variability

Theresa Mathes[1,7], Ian Brooks[2], Sonja Murto[3,4,5], Michael Tjernström[4,5], Julia Kojoj[5,6], Paul Zieger[5,6], John Prytherch[3], Birgit Wehner[7], and Andreas Held[1]

[1]Chair of Environmental Chemistry and Air Research, Technische Universität Berlin, Berlin, Germany
[2]School of Earth and Environment, University of Leeds, Leeds, U.K.
[3]Department of Earth Sciences, Uppsala University, Uppsala, Sweden
[4]Department of Meteorology, Stockholm University, Stockholm, Sweden
[5]Bolin Centre for Climate Research, Stockholm, Sweden
[6]Department of Environmental Science, Stockholm University, Stockholm, Sweden
[7]Department of Atmospheric Microphysics, Leibniz Institute for Tropospheric Research, Leipzig, Germany

Correspondence: Theresa Mathes (mathes@tropos.de)

Abstract. The Arctic is warming at a significantly faster rate than the global average, which is affecting local climate processes. Aerosol particles play a central role by influencing the energy balance directly through the scattering and absorption of solar radiation and indirectly by acting as cloud condensation nuclei. However, the processes that control aerosol concentrations, such as the mechanisms governing vertical particle exchange, are not well understood, particularly over sea ice. During the ARTofMELT campaign in spring 2023, five weeks of continuous eddy covariance measurements of turbulent particle fluxes were conducted in the High Arctic to investigate the spatial and temporal variability of particle sources and sinks over three surface types. Overall, net particle deposition dominated, with median deposition fluxes of $-0.02 \times 10^6\,\mathrm{m^{-2}\,s^{-1}}$ over closed ice. This confirms the role of ice surfaces as a particle sink under low to moderate turbulence. Under strong winds, net particle emission fluxes of up to $0.98 \times 10^6\,\mathrm{m^{-2}\,s^{-1}}$ were observed over closed ice surfaces, which are likely linked to processes involving blowing snow. A mixture of emission and deposition was observed over leads and open water surfaces. These observations highlight how surface heterogeneity and turbulence intensity can influence particle exchange in the High Arctic. As sea ice retreats and the extent of open water increases, local particle sources are expected to become more relevant to Arctic aerosol budgets and cloud processes. The results provide observational constraints on particle fluxes, helping to reduce related uncertainties in Arctic model simulations.

1 Introduction

The Arctic is experiencing climate change at a significantly faster rate than the global average (Rantanen et al., 2022; Westergaard-Nielsen et al., 2018; You et al., 2021; Meredith et al., 2019). Since 1979, warming has occurred two to seven times faster than the global rate, with the most pronounced changes in the Eurasian sector, particularly the Barents Sea region (Rantanen et al., 2022). This accelerated warming, also known as Arctic amplification (e.g., Wendisch et al., 2019), is closely linked to feedback mechanisms in the climate system and has an impact on weather systems and climate worldwide (Cohen et al., 2014). Aerosol

https://doi.org/10.5194/egusphere-2026-1792
Preprint. Discussion started: 8 May 2026

particles, hereafter referred to as particles, play a central role in the Arctic climate system (Arctic Monitoring and Assessment Programme, 2021; Serreze and Barry, 2011). They influence the energy balance directly by scattering and absorbing solar radiation, and indirectly by acting as cloud condensation nuclei or ice nucleation particles. This alters cloud properties, cloud lifetime, and radiation feedback (Twomey, 1977; Albrecht, 1989; Carslaw et al., 2013). Especially in autumn, particle number concentrations can be very low (Tunved et al., 2013). Under these conditions, even small additional sources can become relevant. This applies to both natural and anthropogenic sources. Small changes in particle numbers can influence cloud formation and the radiation balance (Mauritsen et al., 2011). These effects may modify the Arctic radiation budget and thereby influence feedback processes affecting sea ice extent (Stevens et al., 2018). Recent studies show that particles smaller than 70 nm in the Aitken mode can contribute to cloud condensation nuclei under conditions of sufficiently high supersaturation and low accumulation mode particle concentrations (Baccarini et al., 2020; Karlsson et al., 2022). Changes in cloud condensation nuclei availability may in turn influence cloud microphysical properties.

The Arctic is strongly influenced by the long-range transport of anthropogenic aerosols, especially in winter and spring. This phenomenon is known as Arctic haze (e.g., Shaw, 1995). During the summer months, large scale atmospheric circulation patterns shift, reducing the influence of long range transport to the high Arctic. At the same time, more frequent precipitation enhances wet scavenging, leading to lower aerosol particle concentrations in the boundary layer. Consequently, local Arctic sources can play a comparatively more important role (e.g., Schmale et al., 2022; Law and Stohl, 2007; Garrett et al., 2010). These local sources include secondary aerosol formation from marine precursor gases (e.g., Heintzenberg et al., 2015), emissions from open leads and associated sea spray production (e.g., Lapere et al., 2023), terrestrial emissions (e.g., Bullard et al., 2016), and biological sources from both sea ice margins and terrestrial environments (e.g., Moschos et al., 2022; Tobo et al., 2024; Pereira Freitas et al., 2023). However, the individual contributions of these sources to total particle number concentration remain unclear. The climatic relevance of different particle types is not necessarily reflected in their number concentration. Newly formed particles may dominate in number, but their impact on aerosol cloud interactions depends on subsequent growth to sizes large enough to activate as cloud condensation nuclei (e.g., Kulmala et al., 2004; Spracklen et al., 2008). Conversely, ice nucleating particles occur at very low concentrations and can nonetheless exert a strong influence on cloud properties (e.g., Kanji et al., 2017; Creamean et al., 2022). The relative contributions of different sources to total aerosol particle number concentration remain uncertain, which leads to uncertainties when quantifying their regional climate impacts (Song et al., 2022; Chylek et al., 2016).

There are still significant gaps in our knowledge of the processes controlling aerosol abundance in the Arctic, including emissions, transport, transformation, and removal (Korhonen et al., 2008; Willis et al., 2018). These gaps hinder the accurate modeling of aerosol climate interactions. For instance, numerical models cannot yet realistically reproduce the observed aerosol processes in polar regions, partly due to incomplete emission inventories (Whaley et al., 2022; Koike et al., 2025). Furthermore, dry deposition depends on the physical properties of the particles, as well as on meteorological and surface specific factors (Donateo and Contini, 2014; Mohan, 2015; Farmer et al., 2021; Donateo et al., 2023). As Willis et al. (2018) and

https://doi.org/10.5194/egusphere-2026-1792
Preprint. Discussion started: 8 May 2026

Schmale et al. (2021) point out, very few measurements of the turbulent flux of particles and aerosol precursor gases have been taken in the Arctic to date. Such measurements are crucial for modeling aerosol formation and emissions. Therefore, accurate quantification of vertical turbulent particle fluxes is required to enhance our understanding of the local particle budget in the high Arctic (Saylor et al., 2022).

Initial evidence of local aerosol sources over open leads was described by Scott and Levin (1972), and the first quantitative particle flux measurements in the high Arctic were provided by Nilsson and Rannik (2001) and Nilsson et al. (2001). Subsequent measurements were conducted by Held et al. (2011b, a), Donateo et al. (2023, 2025) and Mathes et al. (2025). Comparable measurements also exist from Antarctica (Grönlund et al., 2002; Contini et al., 2010). However, the available measurements are sparse, particularly over sea ice, and additional, more extensive datasets are still required. Conducting eddy covariance measurements poses considerable challenges. On the one hand, a temporal resolution of about 10 Hz is needed to capture small-scale turbulent fluctuations. On the other hand, low particle concentrations and instrumental limitations make detection difficult (Donateo and Contini, 2014). The gradient method is an alternative to eddy covariance. It is based on flux profile relationships and requires a lower instrumental time response but relies upon the assumptions underlying Monin-Obukhov surface layer similarity being valid. (Foken and Mauder, 2024; Held et al., 2011b; Petelski and Piskozub, 2006).

This study examines the spatial variability of particle sources and sinks in the Arctic Ocean. It is based on a continuous eddy covariance dataset covering five weeks of turbulent particle flux measurements in the High Arctic. This is one of the longest datasets of its kind reported for this region. Direct observations of particle exchange between the surface and the atmosphere are still scarce in the Arctic, and the mechanisms influencing vertical particle exchange are not yet fully understood. Fluxes are classified according to three surface types: open water, leads, and closed ice. This allows us to evaluate the impact of surface conditions on particle exchange and identify the circumstances in which the Arctic Ocean surface acts as a net source or sink of particles. The results provide observational data to help reduce uncertainties in Arctic model simulations relating to particle fluxes.

2 Data and Methods

This work is based on data collected during the ARTofMELT (Atmospheric Rivers and the Onset of Arctic Sea Ice Melt) expedition, which took place in the Arctic Ocean in spring 2023 aboard the Swedish icebreaker *Oden*. The primary objective of the campaign was to improve our understanding of the processes that trigger the onset of sea ice melt and to investigate its connection to atmospheric rivers, which carry warm, moist air poleward in narrow corridors (Tjernström and Zieger, 2025; Swedish Polar Research Secretariat, 2024). The expedition embarked from Svalbard on 8 May 2023 and concluded there on 15 June 2023. After departure, *Oden* initially headed north towards the marginal ice zone, where the ship remained for approximately half a day to conduct measurements near the ice edge. Within the marginal ice zone, *Oden* subsequently turned south to around 78° N, before gradually moving west to approximately 4° W. *Oden* then turned northeast to around 81° N and 14° E, followed

https://doi.org/10.5194/egusphere-2026-1792
Preprint. Discussion started: 8 May 2026

by several course changes, before heading south again towards Svalbard. During two ice camps, *Oden* was moored to an ice floe and drifted with the ice. The first ice camp took place from 16 to 21 May at 79.6° N, 1.3°W, the second from 29 May to 11 June at 79.8° N, 2.8° E.

This manuscript presents eddy covariance particle fluxes, which were continuously measured on *Oden´s* foremast between May 10 and June 12. Additional data on particle number concentrations and meteorological parameters were used for data interpretation. Profiles of temperature, humidity, pressure, and wind speed are obtained from radiosonde weather balloons, launched from the Swedish icebreaker Oden (Murto et al., 2024b). Mean near surface meteorological conditions were obtained from a weather station deployed on the 7th top deck of *Oden* (Murto et al., 2024a). The analysis focuses on the potential dependence of turbulent particle fluxes on the surface type. Based on hourly images taken on the foredeck of *Oden*, the surface was divided into three categories:

1. closed ice: smooth snow-covered ice surfaces without ridges or melt ponds (e.g. Fig. 1a);
2. open water: extensive open water and wide lead surfaces (e.g., Fig. 1b);
3. lead: open water within leads or thin ice within pack ice (e.g., Fig. 1c);

Figure 1. Example pictures from the automatic camera showing different dominating surface types: (a) closed ice; (b) open water; (c) leads.

Since *Oden* was typically aligned with the main wind direction for atmospheric measurements, the relative wind direction was most frequently onto the bow (53% of the measurement campaign, 315° to 45°). Wind was onto the port side in 19% of the cases (215 to 314°), and onto the starboard side in 21% of the cases (46° to 145°) (Murto et al., 2024a) The remaining percentage represents wind onto the aft deck, but these periods are typically affected by ship exhaust and discarded from further analysis.

2.1 Sampling methodology

Turbulent particle fluxes were measured by eddy covariance using a sonic anemometer (uSonic-3, Metek, Elmshorn, Germany) and a mixing-type condensation particle counter (MCPC 1720, Brechtel, Hayward, CA, USA). The sonic anemometer measured three-dimensional wind components and sonic temperature at an acquisition rate of 40 Hz. It was installed on the foremast, 20.3 m above the water or ice surface, over the *Oden's* bow (Fig. A1). For particle measurements, an aluminium box

https://doi.org/10.5194/egusphere-2026-1792
Preprint. Discussion started: 8 May 2026

housing the MCPC was installed at the bottom of the foremast (Fig. A1c, d). The box was heated to 15 °C to ensure stable instrument operation, while the sampling lines inside the box were kept as short as possible to reduce residence time and thereby minimize potential evaporation. The inlet of the MCPC sampling line was positioned directly next to the sonic anemometer (Fig. A1e).

Starting at the MCPC box located at the bottom of the foremast, the sampling line consisted of 2.8 m of conductive tubing with an inner diameter of 4.2 mm, connecting the instrument to the mast base. From there, 11.2 m of stainless steel tubing with an inner diameter of 4.5 mm ran upward along the foremast. The final section consisted of 10 cm of conductive tubing with an inner diameter of 6.2 mm, oriented downward to protect the sampling line from precipitation. A bypass system was used due to the long sampling line to obtain a total flow rate of approximately 5.5 l min^{-1} in the sampling line. Part of the flow was diverted around the MCPC via an auxiliary flow path driven by a second vacuum pump, and then recombined downstream (Oehlke, personal communication). This increased the inlet flow velocity and reduced residence time. Butanol was used as the working fluid in the MCPC, and was then removed from the exhaust gas using activated charcoal. The MCPC measured particle number concentrations with a lower cutoff diameter of 7 nm. According to the manufacturer, the nominal response time of the MCPC is 180 ms, which corresponds to a resolution with a frequency of 5.6 Hz. Particle counts were recorded at 20 Hz. The particle number concentration was calculated and corrected using the simultaneously logged 1 Hz particle counts and flow data. The sensible heat flux was calculated using measurements of air temperature and relative humidity taken with an aspirated sensor at the top of the foremast (MP101, Rotronic, Hauppauge, NY, USA).

Hourly images of the ship's surroundings used for classifying the surface types were captured using three cameras (Mobotix M24 IP, Langmeil, Germany) installed on the seventh deck of *Oden*, facing port side, starboard side, and the bow.

2.2 Data Analysis

The measured particle number concentrations were corrected for particle loss occurring in the sampling inlet. In particular, small particles are lost through diffusion to the tubing and inlet walls (Kulkarni et al., 2011). Diffusional losses in a flow through a circular tube with a uniform inlet were calculated for various particle diameters according to Gormley and Kennedy (1949). To determine the penetration fraction of the ambient particle population, the number size distribution of particles between 15 and 792 nm was taken into account. This was measured with a temporal resolution of 12 minutes using a differential mobility particle sizer (DMPS) on the fourth deck of Oden, with an inlet at roughly the same height as the mast. Periods influenced by pollution from the ship's exhaust were excluded based on the derivative of the total particle number, following a similar principle as described by Beck et al. (2022). The calculated penetration efficiency was between 25% for 15 nm particles and 100% for particles from 240 to 792 nm. The mean penetration efficiency for the total particle population was 95%.

Eddy covariance calculations of momentum, sensible heat, and particle fluxes were performed using Eddy Pro software (LI-COR, Inc., 2021). The direction of the turbulent fluxes is defined such that an upward flux is positive and a downward

https://doi.org/10.5194/egusphere-2026-1792
Preprint. Discussion started: 8 May 2026

flux is negative. To determine a suitable averaging period for eddy covariance calculations, ogives (i.e., cumulative cospectra representing the contribution of different frequencies to the total flux) were calculated from 10 Hz eddy covariance data following linear detrending and double rotation of the wind components. To this end, preliminary particle flux calculations and spectral analyses were performed. The mean ogives, averaged over multiple time periods, were normalized to the total particle flux covariance so that they converge to 1 at low frequencies. The choice of an averaging interval was guided by the interpretation of ogive plots, as suggested by Moncrieff et al. (2005). As shown in Figure 2a, most of the turbulent contributions to the flux are captured within 5-minute periods. An averaging interval of 20 minutes was selected. This allows slightly larger turbulent eddies to be included. At the same time, slower variations that are not related to local turbulent exchange are not considered.

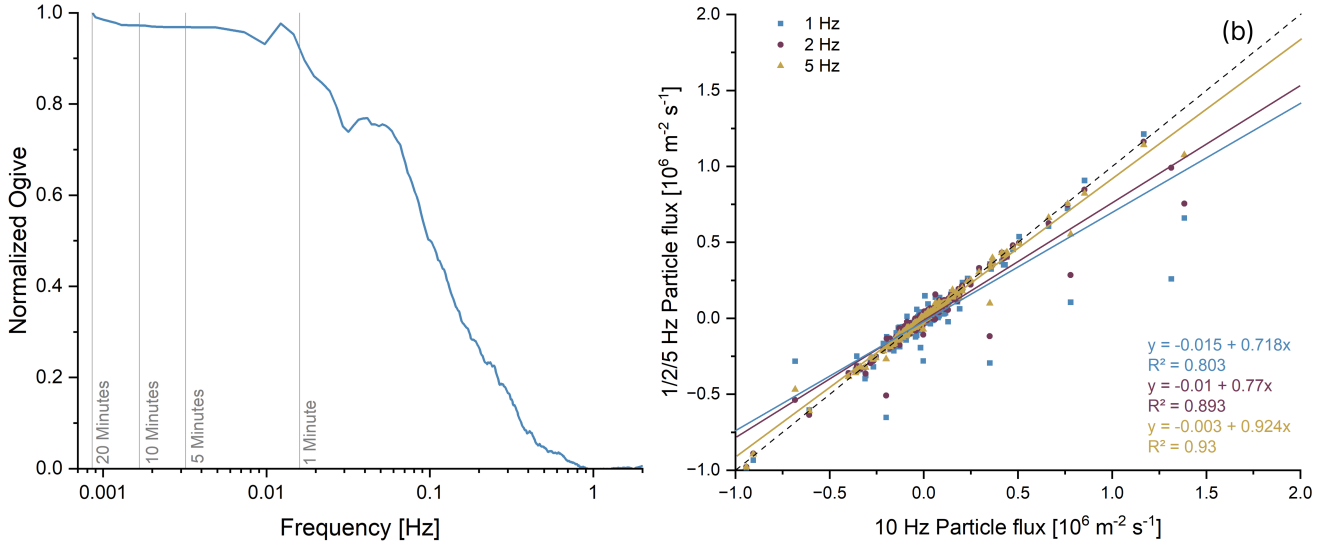

Figure 2. Normalized mean ogive for the particle flux (a), calculated from 10 Hz eddy covariance data. The vertical lines show the frequencies corresponding to 20, 10, 5, and 1-minute intervals. Scatter plot (b) of particle number fluxes calculated using 10 Hz data (on x-axis) and 1, 2, 5 Hz (on y-axis), and linear regressions. The dashed line indicates the 1:1 slope.

According to the manufacturer, the MCPC's response time corresponds to an effective frequency of approximately 5.6 Hz. Figure 2b illustrates the systematic reduction in turbulent particle fluxes with lower time resolution of 1, 2, and 5 Hz compared to 10 Hz data, as indicated by the slope of the linear regression functions. Here, it becomes clear that the regression slope shows a difference between 5 and 10 Hz, with the 5 Hz data points with an R^2 of 0.93 being closest to the 1:1 curve. This suggests that the MCPC can measure small-scale turbulent fluctuations of at least 5–10 Hz and that its time response is likely to be within this range. A comparison of the theoretical flux reduction (18% at 1 Hz, 8% at 2 Hz, and 2% at 5 Hz) according to Horst (1997) shows qualitative agreement with the experimental reductions of 29%, 23%, and 8% indicated by the slopes of the linear regression functions. The high-frequency losses were corrected after Horst (1997).

https://doi.org/10.5194/egusphere-2026-1792
Preprint. Discussion started: 8 May 2026

For the eddy covariance calculations, the particle counts and wind data were averaged at a frequency of 10 Hz. This temporal resolution captures small-scale turbulent fluctuations in the 5–10 Hz frequency range, while remaining consistent with the effective time response of the MCPC.

Turbulent wind measurements made from the foremast of a ship require correction for both their changing orientation and the motion of the platform. 3-axis accelerations and rotation rates were measured at 40 Hz at the base of the sonic anemometer on the foremast (MTi-G-700, XSens, Enschede, NL) and combined with low frequency ship navigation data to calculate corrections for the orientation and motion of the anemometer (Edson et al., 1998; Prytherch et al., 2015). Distortion of the mean flow over the ship's superstructure is corrected using the results of a CFD modeling study of Oden (Moat and Yelland, 2015; Prytherch et al., 2017).

After motion correction, double rotation was applied to align the coordinate system with the mean flow streamlines and to ensure a zero mean vertical wind velocity (Wilczak et al., 2001). Linear detrending over 20 minutes was used as the detrending method (Moncrieff et al., 2006). Standard statistical tests from Vickers and Mahrt (1997) were applied for raw data screening. In addition, spike count and removal procedures following Mauder et al. (2013) were used. A tolerance level of 1% was set for accepted spikes and dropouts. As the eddy covariance fluxes were measured using a closed-path instrument, it was necessary to determine the time lag between fluctuations in the vertical wind component and particle concentration. Based on the pipe length and inner diameter of the inlet tubing, the total inlet tubing volume was estimated to be 0.22 l. With a volume flow rate of 5.5 l min^{-1}, the resulting theoretical travel time is approximately 2.4 s. An additional residence time of approximately 0.6 s within the MCPC was included. This results in an estimated total time lag of 3 s, which was confirmed by covariance maximization.

Data contaminated by ship exhaust were removed. To this end, the relative wind direction with respect to the ship's bow, the particle concentration measured at the foremast using an MCPC, and the particle concentration measured using a CPC in the aerosol container on the fourth deck were evaluated. First, the MCPC and CPC concentrations were averaged to a time resolution of one minute. A "wind alarm" was triggered when the relative wind direction onto the bow was outside the clean sector of 270° to 90°. A "concentration alarm" was triggered when the CPC in the aerosol container exceeded a threshold concentration. This threshold varied throughout the expedition depending on the ambient background concentration. The following pollution cases were thus defined:

Case A: At least one alarm was active. The particle concentration of the MCPC exceeded 200 cm^{-3} and was at least 10% higher than the 20-minute mean concentration of the MCPC.

Case B: At least one alarm was active, and the absolute difference between the particle concentration of the MCPC and the CPC in the aerosol container was less than 200 cm^{-3}; the MCPC was more than 20% above the 20-minute mean concentration.

Case C: At least one alarm was active, and the particle concentration of the MCPC exceeded 800 cm^{-3}.

https://doi.org/10.5194/egusphere-2026-1792
Preprint. Discussion started: 8 May 2026

Case D: The MCPC concentration exceeded 2,000 cm^{-3}, regardless of any alarm status.

An additional 10-second interval was removed before and after each pollution case to ensure that the polluted air parcel was not included in the analysis. 20-minute averaging intervals containing more than 10% missing data were discarded. Data gaps were not replaced or interpolated. In total, 17% of the entire measurement data were affected by pollution (including the 10-second buffer) and were removed. Within the fraction of the measurement data affected by pollution, Cases A and C occurred most frequently, at 32% and 58%, respectively.

The surrounding surface types were automatically evaluated using a random forest algorithm (Waikato Environment for Knowledge Analysis (WEKA)) applied to hourly images. This was done in combination with macros of the image processing program ImageJ (Schneider et al., 2012) and the image processing package Fiji. ImageJ was used to tilt, crop, and resize the images. The images were then manually classified according to various features. WEKA on Fiji was subsequently employed to train different models for image segmentation. The next step was to use macros to automate the segmentation of images in batches using WEKA models. Finally, ImageJ was used to calculate the area ratio of the segmentation into closed ice surfaces, water surfaces, and mixed surfaces consisting of thin ice and brash ice (Fig. 3). Depending on the relative direction of the wind in relation to the ship's position, one of three image orientations was selected to define the surface type located upstream. The data on the relative wind direction was also averaged over a period of one hour. The analysis was manually checked, as the algorithm occasionally misclassified surface types in images affected by fog, water droplets on the camera, or small waves. This made it difficult to distinguish small ice floes from white caps.

To avoid missclassification due to changing surface types, surface type data should be considered with caution for periods of maneuvering, icebreaking and/or when the speed over ground was larger than 1 knot. For the statistical evaluation of the surface type fraction, only periods during which *Oden* was drifting with a low speed over ground $\leq$ 1 knot were considered. Taking into account this criterion, approximately 75% of the dataset remained available for analysis.

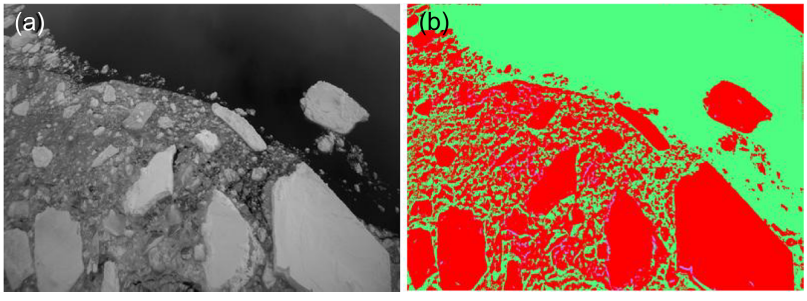

Figure 3. Example of surface type characterization, showing the (a) cropped camera image and the (b) analyzed surface types. Thick ice is displayed in red, open water in green, and thin ice in purple.

Particle fluxes are influenced not only by surface type but also by the particle number concentrations (Nilsson and Rannik, 2001), as well as by micrometeorological conditions such as turbulence development and atmospheric stability. The friction

https://doi.org/10.5194/egusphere-2026-1792
Preprint. Discussion started: 8 May 2026

velocity (u_*), is a measure of turbulence at the surface:

$$u_* = \left[(\overline{u'w'})^2 + (\overline{v'w'})^2 \right]^{\frac{1}{4}} \tag{1}$$

u and v are the horizontal wind components, w is the vertical wind component. The prime denotes the fluctuation about the mean value, and the overbar denotes the average. The dimensionless parameter $\zeta = z/L$ was used to characterize atmospheric stability, where z is the height and L is the Obukhov length:

$$L = -\frac{{u_*}^3}{\kappa \frac{g}{T} \overline{w'T'}} \tag{2}$$

where κ is the von Karman constant (= 0.40), g is the gravitational acceleration (= 9.81 m s^{-2}), $\overline{w'T'}$ is the covariance of the turbulent fluctuations of vertical wind speed w and sonic temperature T. Positive values for the stability parameter z/L indicate stable stratification, negative values refer to unstable conditions, and neutral stratification is given by a value close to zero (Sorbjan and Grachev, 2010).

The measured particle fluxes represent a combination of emission and deposition of particles, with positive net fluxes dominated by emission and negative net fluxes by deposition. To separate deposition from potential emission contributions to the measured net particle fluxes, the dry deposition velocity of aerosol particles was calculated, using a size resolved resistance model following Zhang et al. (2001) and Emerson et al. (2020). The approach combines gravitational settling with turbulent transfer through the atmospheric surface layer and surface uptake processes. The model was applied for smooth surfaces representative of closed ice, leads, and open water. The modeled deposition velocity $V_D(D_p)$ for particles of diameter D_p is given by:

$$V_D(D_p) = v_g(D_p) + \frac{1}{R_a + R_s}, \tag{3}$$

where v_g is the gravitational settling velocity, R_a is the aerodynamic resistance, and R_s is the surface resistance. Model parameters are summarized in Table A1. The aerodynamic resistance was calculated as:

$$R_a = \frac{\ln(z/z_0)}{\kappa u_*} \phi_H(z/L), \tag{4}$$

where z_0 is the surface roughness length. A z_0 = 0.0002 m (e.g., Nilsson and Rannik, 2001; Held et al., 2011a; Andreas et al., 2010) representative of closed ice surfaces was applied for all surface types. In (Held et al., 2011a), z_0 values ranged from 0.00001 m to 0.01 m. Sensitivity tests show that varying z_0 within this range changes the calculated deposition velocity by about 5%, therefore the value z_0 = 0.0002 m was used for all surface types. ϕ_H is a stability correction function depending on the stability parameter z/L. Stability corrections follow standard Businger-Dyer formulations, and extreme values of z/L were limited to the range $[-5, 5]$ for numerical stability. The surface resistance was calculated as:

$$R_s = \frac{1}{e_0 \, u_* \, (E_B + E_{IM} + E_{IN}) \, R_1}, \tag{5}$$

https://doi.org/10.5194/egusphere-2026-1792
Preprint. Discussion started: 8 May 2026

where e_0 is an empirical constant and E_B, E_{IM}, and E_{IN} represent collection efficiencies due to Brownian diffusion, inertial impaction, and interception, respectively. The term $R_1 = \exp(-\sqrt{St})$ accounts for reduced collection efficiency at low Stokes numbers, with the Stokes number defined as:

$$St = \frac{v_g u_*^2}{\nu}, \tag{6}$$

where ν is the kinematic viscosity of air. In contrast to the original formulation by Zhang et al. (2001), the Brownian diffusion efficiency was parameterized following Emerson et al. (2020), using:

$$E_B = C_B\, Sc^{-\gamma}, \tag{7}$$

where Sc is the Schmidt number and C_B and γ are constants, adopted to better represent particle transfer over smooth ice and water surfaces (Tab. A1). The Schmidt number was calculated as:

$$Sc = \frac{\nu}{D}, \tag{8}$$

where ν is the kinematic viscosity of air and D is the particle Brownian diffusivity. The inertial impaction efficiency was calculated as:

$$E_{IM} = \frac{St^2}{400 + St^2}, \tag{9}$$

Particle loss due to interception (E_{IN}) is not taken into account because in the applied model, interception is only parametrized for surfaces with collectors, which is not applicable for ice and water surfaces (Zhang et al., 2001; Emerson et al., 2020). The gravitational settling velocity was calculated assuming Stokes flow with Cunningham slip correction. Air viscosity, density, and mean free path were computed as functions of temperature and pressure. The size-resolved deposition flux for each diameter bin was calculated as:

$$F_{\text{dep},i} = -v_d(D_{p,i})\, C, \tag{10}$$

where C is the particle number concentration in size bin i, taken from the DMPS measurements on the fourth deck. The total modeled deposition flux was obtained by summing over all size bins from 15 nm to 792 nm. The inferred emission strength was defined as the difference between the measured net particle flux and the modeled deposition flux. Positive values indicate periods during which particle emission at the surface is inferred. Negative values indicate periods during which the measured net particle flux is smaller than the modeled dry deposition, which may reflect uncertainties in the flux or deposition estimates.

3 Results and Discussion

The following section first describes the meteorological conditions during the expedition, as well as the particle number concentration and the temporal variation of surface types (Sect. 3.1). It then goes on to discuss the different surface types in detail, as well as their influence on the particle flux (Sect. 3.2), the inferred particle emission strength (Sect. 3.3) and net particle emission events during high wind speed events (Sect. 3.4).

https://doi.org/10.5194/egusphere-2026-1792
Preprint. Discussion started: 8 May 2026

3.1 General overview

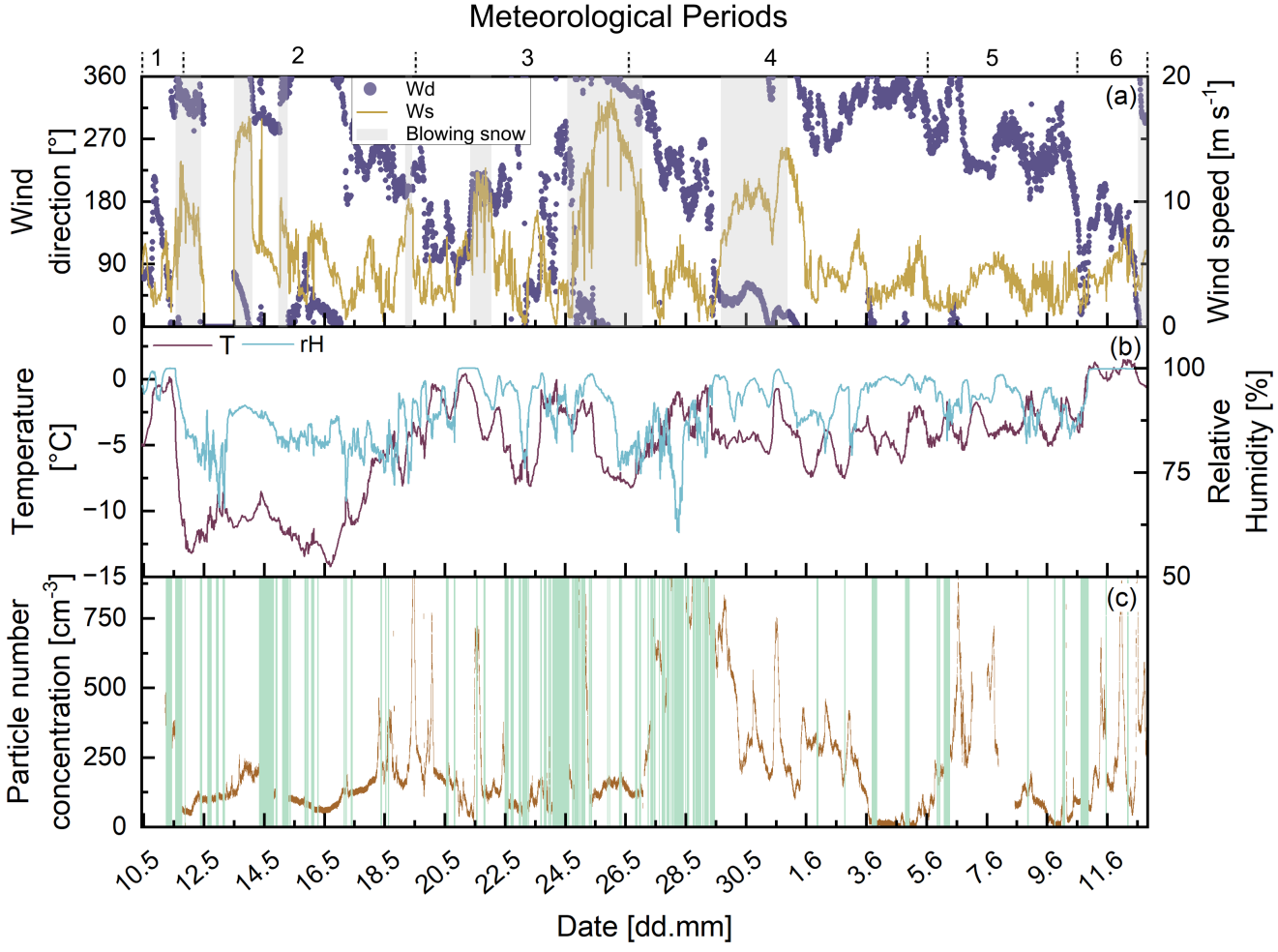

Figure 4. Overview of the six meteorological periods defined in Murto et al. (2024a) and Murto and Tjernström (2024), for the entire measurement period, from 10 May to 12 June 2023, with (a) wind direction (Wd, purple, in °) on the left y-axis and wind speed (Ws, beige, in m s^{-1}) on the right y-axis. Meteorological data are shown as 10-minute averages. The high wind speed periods are shown in grey. Panel (b) shows the temperature (T, brown, in °C) on the left axis and the relative humidity (rH, blue, in %) on the right axis. Panel (c) shows the particle number concentration (cm^{-3}), with pollution periods marked in turquoise.

Based on radiosonde data, air mass trajectories, wind direction, and wind speed, the measurement period can be divided into six periods (Murto and Tjernström, 2024; Murto et al., 2024a, b). For the first one and a half days, up until the morning of 11 May, it was mild and moist, with temperatures around -2°C and winds blowing from the southeast (Fig. 4a and b). Period 2, until 19 May, was characterised by low temperatures down to -14°C and northwesterly/northeasterly winds. Period 3, until 26 May, was mild and moist again. The first temporary warming occurred on 20 May, when temperatures rose above 0 °C and

https://doi.org/10.5194/egusphere-2026-1792
Preprint. Discussion started: 8 May 2026

southerly winds predominated. In Period 4 until 5 June, northerly winds predominated, accompanied by fluctuating temperature and humidity. The following period, until 10 June, has temperatures near the melting point again, with warm, dry air aloft and westerly winds. Melt onset occurred on 10 June in the early morning around 06:00 UTC, in period 6, accompanied by rain and southerly winds. In total, eight high wind speed periods with durations of at least four hours were identified during the campaign. These periods were defined as time intervals during which blowing snow could potentially occur. Blowing snow cannot be described by a single fixed wind speed threshold (Fig. A2), as the threshold varies with temperature and snow properties. Warmer snow increases cohesion, while very cold snow increases friction, both leading to higher threshold wind speeds (Li and Pomeroy, 1997). Therefore, a critical threshold derived from air temperature and wind speed using an empirical model was calculated (Li and Pomeroy, 1997). These periods are indicated by grey shading in Fig. 4a. The longest continuous high wind speed period occurred between 24 and 26 May, during which wind speeds reached up to 19 m s^{-1} (10-minute average).

After excluding pollution periods, the average particle concentration for the entire period from 10 May to 12 June 2023 is 220 cm^{-3}. Days with particularly high concentrations are 27 May to 29 May, when the daily average is between 500 and 750 cm^{-3} (Fig. 4c). Conversely, periods with particularly low concentrations are 15 May and 3 and 4 June, with daily averages between 20 and 80 cm^{-3}. The particle size distribution indicates a characteristic transition from Arctic haze to less polluted conditions in late May. Before 26 May, there is a pronounced accumulation mode, with particle concentrations peaking at diameters around 110 nm. This is subsequently replaced by a dominant Aitken mode, with a maximum concentration near a diameter of 50 nm. Also, periods of high wind speed on 13 May, 24 to 26 May, and 31 May coincide with elevated particle number concentrations. Strong winds can enhance sea salt aerosol production through processes such as sea spray and sublimation of blowing snow (Heutte et al., 2025; Ranjithkumar et al., 2025). However, increased concentrations may also reflect transport of marine aerosol from open water (Lapere et al., 2024). The higher concentrations on 12 June could be linked to the onset of melting, as melt-related surface changes have been suggested to enhance aerosol production in the high Arctic (e.g., Pereira Freitas et al., 2025; Mirrielees et al., 2024). Low particle concentrations occur during periods 2 and 4, which are characterized by lower temperatures (especially during period 2) and northerly winds. Air masses from the northern Arctic often contain relatively few aerosol particles due to the scarcity of local sources over the pack ice and deposition losses during transport.

The hourly surface type distribution based on the camera images over the full measurement period (Figure 5a) shows that closed ice was most common at the beginning of the campaign and during the second ice camp from 29 May to 11 June. In contrast, during the first ice camp from 16 to 21 May, surface conditions varied more strongly, with mixed or rapidly alternating types. Overall, closed ice dominates on roughly two-thirds of the 34 measurement days. This high proportion is partly related to the ice camps (shaded in beige in Figure 5d), during which *Oden* was typically surrounded by closed ice, resulting in a stronger influence of closed ice conditions, although open water was occasionally present.

https://doi.org/10.5194/egusphere-2026-1792
Preprint. Discussion started: 8 May 2026

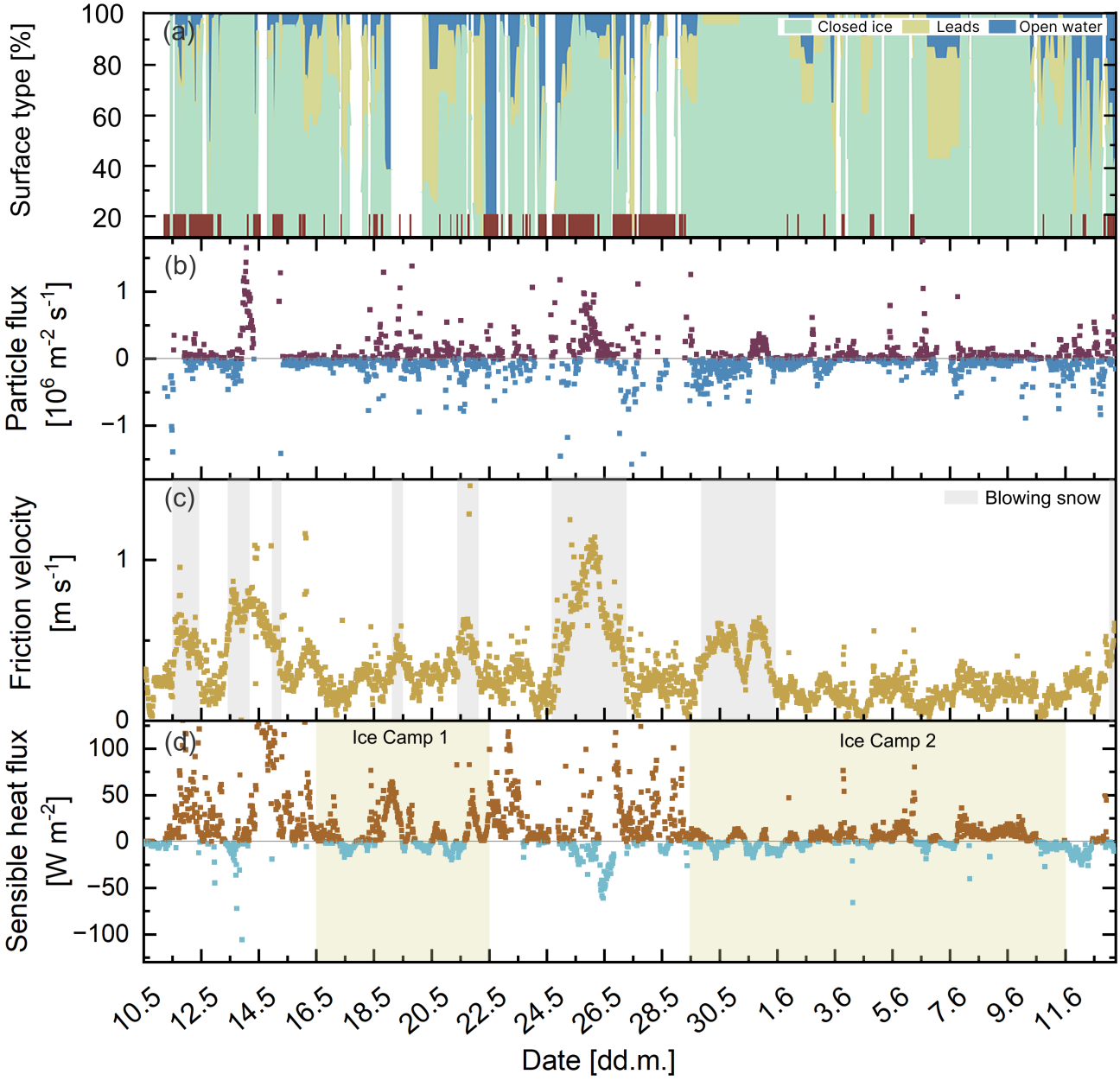

Figure 5. Overview of the surface types, particle and sensible heat fluxes as well as the friction velocity for the entire measurement period, from 10 May to 12 June 2023. The top panel (a) shows the hourly distribution of the three surface types: closed ice (turquoise), leads (beige), and open water (blue). Periods with ship speeds $\geq$ 1 kn are indicated in red. The second panel (b) shows the particle flux (in 10^6 m^{-2} s^{-1}) evaluated in 20-minute intervals. Blue represents net particle deposition, and red represents net particle emission. The third panel (c) shows the friction velocity (u_*, in m s^{-1}) in beige and the high wind speed periods are shown in grey. The bottom panel (d) shows the sensible heat flux (W m^{-2}) evaluated in 20-minute intervals and the periods of the two ice camps (beige shading).

https://doi.org/10.5194/egusphere-2026-1792
Preprint. Discussion started: 8 May 2026

Over the entire expedition, the median 20-minute net particle flux was $-0.02 \times 10^6\,\mathrm{m^{-2}\,s^{-1}}$ (Fig. 5b). This overall net deposition results from a slightly larger proportion of net deposition intervals (58 % of 20-minute intervals). Long, strongly pronounced continuous emission periods occur, for example, on 13 May and 25 May, with median particle fluxes of $0.76 \times 10^6\,\mathrm{m^{-2}\,s^{-1}}$ and $0.48 \times 10^6\,\mathrm{m^{-2}\,s^{-1}}$, respectively. For extended net deposition, an example is the period from 29 May to 31 May, with a median net particle flux of $-0.14 \times 10^6\,\mathrm{m^{-2}\,s^{-1}}$.

Previous studies have shown that strength and direction of the sensible heat flux (Fig. 5d) are closely related to the surface type. Low or negative fluxes are typically observed over closed ice, whereas higher positive fluxes occur over open water (e.g., Held et al., 2011b; Mathes et al., 2025). The increased upward fluxes can be explained by the temperature gradient between the relatively warm water surface (close to the freezing point) and the colder air above. In contrast, thick pack ice has a strong insulating effect, limiting heat exchange with the underlying ocean. Surface temperatures are therefore lower, and sensible heat fluxes are reduced (Held et al., 2011b). Figures 5a and d show that enhanced upward sensible heat fluxes coincide with periods of leads and open water. Strongly negative sensible heat fluxes during high wind speed events suggest heat is being transferred from the atmosphere to the ice surface. This is likely associated with the advection of warmer air masses over the colder ice surface. Higher wind speeds enhance turbulent exchange, thereby increasing the flux. During these periods, turbulent heat fluxes largely control the energy exchange at the surface. On average, sensible heat fluxes are close to zero over the full annual cycle (Tjernström et al., 2012), indicating that they are not controlled by surface type alone but also by seasonal and atmospheric variability.

The net particle flux is strongly influenced by the intensity of turbulence, which is measured by the friction velocity u_* (e.g., Donateo et al., 2023; Grönholm et al., 2009). The median value of u_* is 0.26 ($\pm$ 0.20) $\mathrm{m\,s^{-1}}$ across the entire campaign (Fig. 5c). Days of high absolute particle fluxes coincide with periods of particularly high friction velocities (Fig. 6a). A linear regression analysis of the centers of six friction velocity bins (u_*) and the net particle flux reveals a strong correlation, with an R value of 0.88 (Fig. 6a). The bins were defined based on u_*, with the first bin covering $u_* \leq 0.2$ $\mathrm{m\,s^{-1}}$ and the last bin covering $u_* > 0.8$ $\mathrm{m\,s^{-1}}$, while the remaining boundaries were evenly spaced in between. The relationship between wind speed and net particle flux was analyzed in the same way. The absolute net particle fluxes within the wind speed bins are varying (Fig. 6b), and the linear regression using the bin centers yields a correlation coefficient of R = 0.62. This suggests that higher wind speeds are generally associated with stronger particle fluxes, although the linear relationship is weaker than for friction velocity (more on this in Section 3.4).

https://doi.org/10.5194/egusphere-2026-1792
Preprint. Discussion started: 8 May 2026

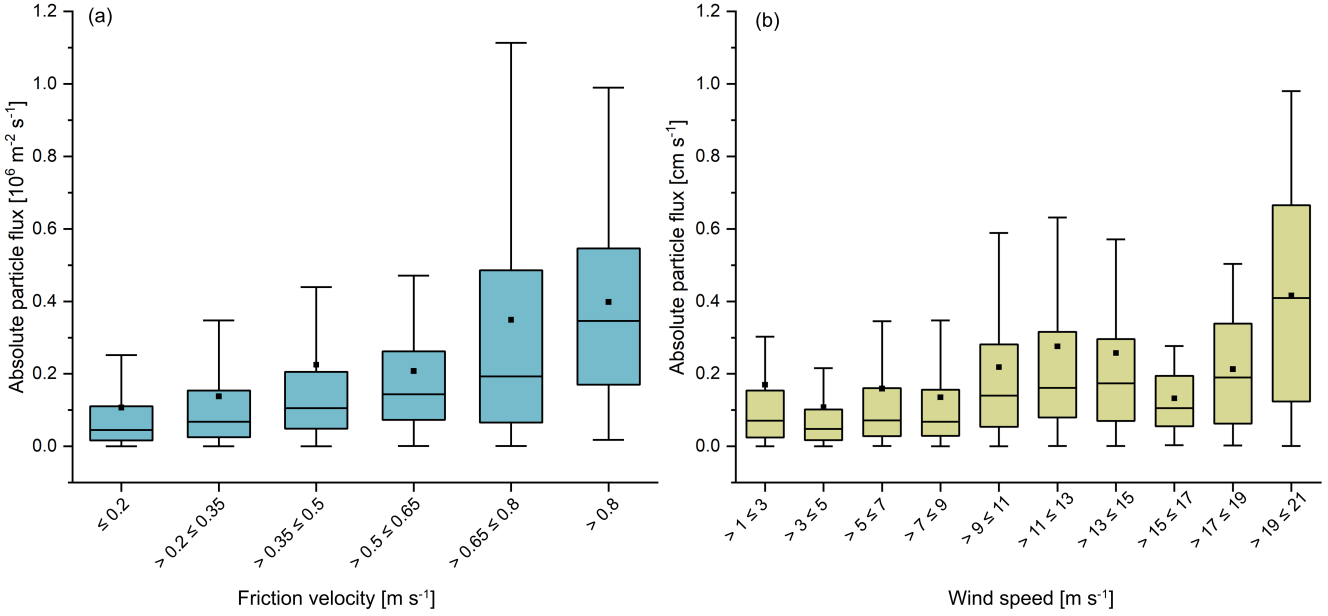

Figure 6. (a) Relationship between friction velocity (m s^{-1}) in different size bins and absolute net particle flux (in 10^6 m^{-2} s^{-1}). (b) Relationship between wind speed (m s^{-1}) in different size bins and net absolute particle flux (in 10^6 m^{-2} s^{-1}). The box represents the 25th to 75th percentiles, while the whiskers indicate the 1.5 interquartile range. The horizontal line denotes the median, and the black square represents the mean.

The stability parameter z/L shows that weakly unstable conditions (-0.2 < z/L < -0.02) dominated the measurement campaign. These conditions occurred in 34% of the 20-minute flux intervals, which is consistent with other observations from Arctic ice camps during late winter. A wide range of stability regimes, including weakly unstable conditions, are reported during winter (e.g., Grachev et al., 2005). Neutral conditions (-0.02 < ζ < 0.02) were also common and occurred in 30% of the intervals. Weakly stable conditions (0.02 < ζ < 0.2) were much less common, occurring in 19% of the intervals. There was no clear correlation between the observed particle fluxes and atmospheric stability conditions.

3.2 Particle fluxes - dependence on surface type

On 23 out of 34 measurement days, the particle flux measurements were primarily influenced by closed ice. On five other days, half of the surface was covered with closed ice. Previous studies have shown that the net particle flux over closed ice surfaces is often directed to the surface, indicating that closed ice surfaces act as particle sinks (e.g., Held et al., 2011a; Donateo et al., 2023). Taking into account all intervals in which closed ice covers more than 70% of the surface, the median net particle flux is $-0.02 \times 10^6\,\mathrm{m^{-2}s^{-1}}$. From 29 May to 2 June, *Oden* was mostly surrounded by closed ice during the second ice camp (Fig. 5a). During this time, the particle flux was dominated by net deposition, except on 31 May (Fig. 5b).

https://doi.org/10.5194/egusphere-2026-1792
Preprint. Discussion started: 8 May 2026

Comparing the net particle fluxes over closed ice with other studies over the same surface type shows that they span a wide range of magnitudes (Fig. 7). For instance, fluxes ranging from -0.08 to $0.05 \times 10^6\,\mathrm{m^{-2}\,s^{-1}}$ were observed at closed ice surfaces in the Arctic using the eddy covariance method (Donateo et al., 2023; Held et al., 2011a; Nilsson and Rannik, 2001). Net particle fluxes using the gradient method are -0.16 to $0.12 \times 10^6\,\mathrm{m^{-2}\,s^{-1}}$ (Held et al., 2011b; Mathes et al., 2025). In Antarctica, median fluxes ranged from -3.33 to $2.75 \times 10^6\,\mathrm{m^{-2}\,s^{-1}}$ (Grönlund et al., 2002). Direct comparisons of flux magnitudes between studies should be made with caution. Strong fluxes often represent individual (e.g., a single 20-minute averaging period) measurements. When averaging or calculating medians, positive and negative fluxes tend to cancel each other out, resulting in values closer to zero.

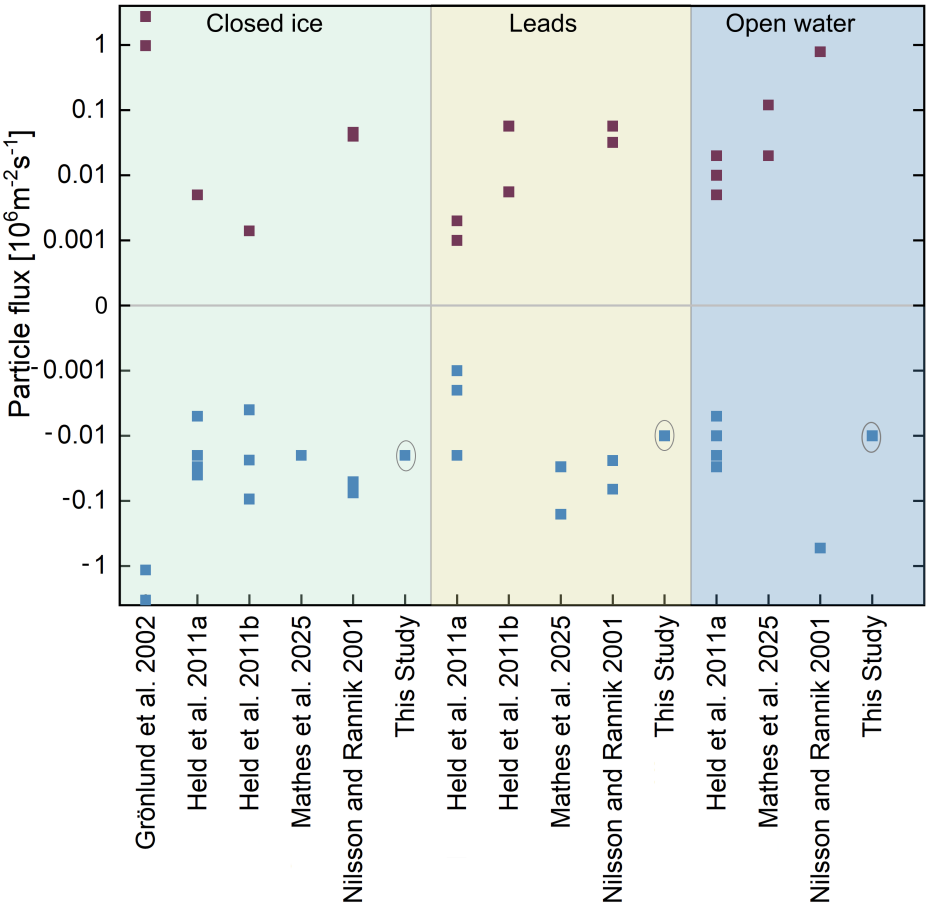

Figure 7. Overview of particle fluxes (10^6 $\mathrm{m^{-2}\ s^{-1}}$) of this study and comparable studies, depending on the surface type. Positive fluxes indicate net emission (red), whereas negative fluxes indicate net deposition (blue). The three background colors indicate the surface types closed ice, leads, and open water. The grey circles highlight the results from this study.

Existing literature makes little distinction between open water, wide, and narrow leads. As the flux footprint may extend beyond the lead, the effective footprint depends on the lead width, limiting the attribution to one specific surface type. Various

https://doi.org/10.5194/egusphere-2026-1792
Preprint. Discussion started: 8 May 2026

explanations have been proposed for the formation of particles in connection with leads. Bubble bursting has been observed at wind speeds of around 4 m s^{-1} and above (May et al., 2016; Kirpes et al., 2019). However, Held et al. (2011a) demonstrated that measurable particle emission fluxes can also occur at low wind speeds. This suggests that emissions from leads and open water are not exclusively driven by wind. The formation of marine aerosols without wind influence has been well documented, including in the high Arctic (Leck et al., 2002). Bubble formation can also occur independently of wind speed. Possible mechanisms include the nucleation of microbubbles at low supersaturation levels, their stabilisation by surfactants, and the formation of subsurface bubble layers that can be detected acoustically. These processes can result in bubbles bursting more slowly at the interface between air and sea. Freezing and melting processes, as well as the release of biogenic gases, may further support these mechanisms (Johnson and Wangersky, 1987; Mulhearn, 1981). This is consistent with earlier reports of aerosol emission over open leads without visible bubble activity (Scott and Levin, 1972). It is also in agreement with observations of bubbles in the surface waters of leads occurring under weak wind conditions and thin ice cover (Norris et al., 2011). In the open ocean, wind-driven breaking waves typically produce bubble clouds that extend a few meters below the surface (e.g., Anguelova and Huq, 2012). These conditions also promote the selective uptake of high molecular weight organic matter into sea spray droplets (Farmer et al., 1993). White caps in pack ice regions tend to be smaller and occur less frequently than in the open ocean. This may explain the comparatively weak net emission observed over leads and open water during this campaign, where the median particle flux is close to zero. This suggests that, although such emission events are possible, they do not dominate the overall particle exchange between the surface and the atmosphere.

Quantitatively, the magnitude and sign of the fluxes observed in this study are in good agreement with earlier measurements. Held et al. (2011a) reported an almost equal number of net emission and deposition events associated with open water. The observed fluxes ranged from $-0.03 \times 10^6\,\mathrm{m^{-2}\,s^{-1}}$ to $0.02 \times 10^6\,\mathrm{m^{-2}\,s^{-1}}$ (Fig. 7b). These closely match the near zero median fluxes obtained here. Both positive and negative fluxes across leads were also observed by Nilsson and Rannik (2001). The median value of positive fluxes near leads was $0.79 \times 10^6\,\mathrm{m^{-2}\,s^{-1}}$, while the median value of negative fluxes was $-0.53 \times 10^6\,\mathrm{m^{-2}\,s^{-1}}$ (Nilsson and Rannik, 2001).

https://doi.org/10.5194/egusphere-2026-1792
Preprint. Discussion started: 8 May 2026

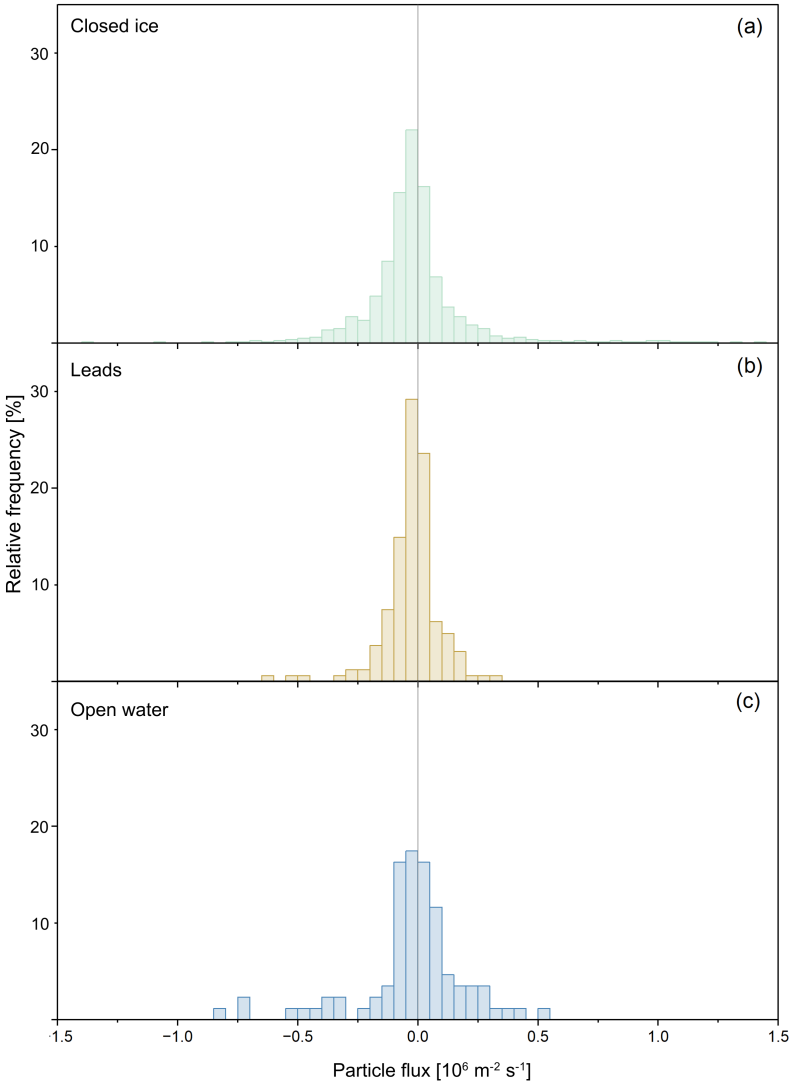

Figure 8. Relative frequency distributions of particle number fluxes (in $10^6\,\mathrm{m}^{-2}\,\mathrm{s}^{-1}$) for the three surface types: (a) closed ice, (b) leads, and (c) open water. The vertical grey line indicates zero flux, separating net particle deposition from net particle emission. Only stationary periods with ship speed ≤ 1 kn are included.

For narrow leads, Held et al. (2011a) reported fluxes in a similar range from $-0.02 \times 10^6\,\mathrm{m}^{-2}\,\mathrm{s}^{-1}$ to slightly positive values using the eddy covariance method. In contrast, fluxes determined using the gradient method were all positive but limited to a few selected periods (Held et al., 2011b). The flux reported by Nilsson and Rannik (2001) for leads ranged from -0.07 to $0.06 \times 10^6\,\mathrm{m}^{-2}\,\mathrm{s}^{-1}$ (Fig. 7b). When both positive and negative fluxes are considered, the net flux is found to be close to zero (Nilsson and Rannik, 2001). However, as each value represents the net flux, this does not imply an absence of emissions, but rather that emission and deposition events balance each other out. This is consistent with the dominance of weak deposition or

https://doi.org/10.5194/egusphere-2026-1792
Preprint. Discussion started: 8 May 2026

median flux values close to zero observed in this campaign. Willis et al. (2018) and May et al. (2016) state that the strongest net emission particle fluxes occur most frequently in the vicinity of seawater, although fluxes from leads are an order of magnitude lower than those over the open ocean. Model simulations suggest that leads contribute between 0.3% and 3% to the annual locally emitted sea salt particle flux (Lapere et al., 2024).

The relative frequency distribution of particle number fluxes over closed ice (Fig. 8a) shows that the particle flux is dominated by deposition, accounting for about 70% of all intervals. The largest contribution (approximately 22%) is associated with weak deposition close to zero, with fluxes between 0 and $-0.025 \times 10^6\,\mathrm{m}^{-2}\,\mathrm{s}^{-1}$. Taking into account all intervals in which leads covered more than 50% of the surface (approximately 7% of the total measurement period), net deposition was dominant with a median flux of $-0.01 \times 10^6 \mathrm{m}^{-2}\mathrm{s}^{-1}$ (Fig. 8b). Taking into account all intervals in which open water covered more than 50% of the surface (approximately 5% of the total measurement period), the median net particle flux was $-0.01 \times 10^6 \mathrm{m}^{-2}\mathrm{s}^{-1}$. Positive and negative flux intervals occurred in nearly equal numbers (Fig. 8c). This indicates that although open water surfaces can act as a particle source, their overall contribution to particle emission is limited during the campaign. A substantial fraction of open water periods was removed from the dataset, since *Oden* was typically underway when open water was present, and surface type evaluation was restricted to slow movement of the vessel. As a result, particle fluxes associated with open water are likely underrepresented in the filtered dataset. These results place the observed fluxes over leads and open water in a regime characterized by weak net exchange and substantial variability, a behavior that is consistent with previous studies.

3.3 Inferred particle emission strength

The inferred emission strength is defined as the difference between the measured net particle flux and the modeled deposition flux. Positive values indicate the estimated particle emission at the surface. Negative values are caused by either model uncertainty or scatter noise in the individual net flux estimates. Figures 9a-c show the relative and cumulative frequency distributions of the inferred emission strength categorized by surface type and by periods with and without potential blowing snow.

Over closed ice (Fig. 9a), high wind speed conditions are associated with a shift in inferred emission strength towards higher values. During periods when the threshold for blowing snow was not exceeded, the distribution is centered around zero and dominated by weak inferred emission. In contrast, periods with high winds show a higher frequency of positive inferred emission strengths. These results suggest a stronger particle emission relative to deposition under high wind speed conditions. This behavior is also reflected in the cumulative frequency distributions. Together, the results in Figure 9a demonstrate that high wind speed conditions are primarily associated with enhanced inferred particle emission over closed ice. For leads (Fig. 9b), only a small number of intervals meet the blowing snow threshold. This reflects limited sampling during high wind speed conditions, as measurements during storm events were predominantly conducted over closed ice. Consequently, few high wind cases are available for leads, and the effect of blowing snow on inferred emission strength cannot be robustly assessed. For open water (Fig. 9c), blowing snow is not relevant, and none of the intervals exceed the blowing snow threshold.

https://doi.org/10.5194/egusphere-2026-1792
Preprint. Discussion started: 8 May 2026

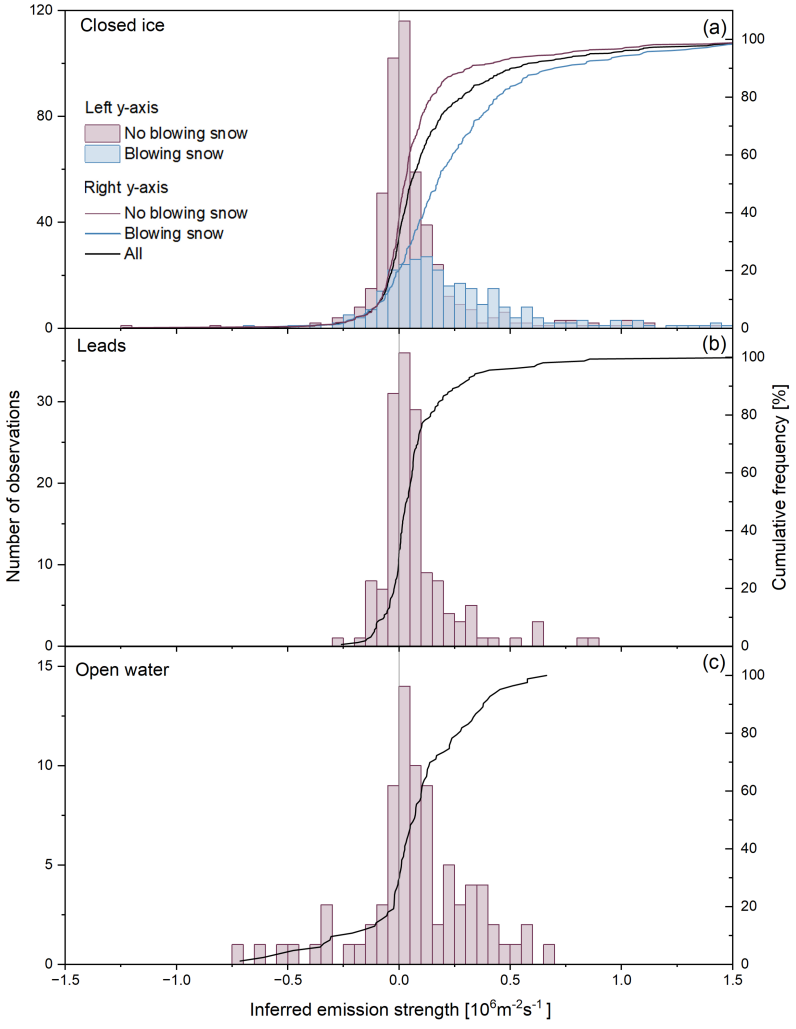

Figure 9. Relative and cumulative frequency distributions of inferred emission strength (in 10^{6-2-1}) for the three surface types: (a) closed ice, (b) leads, and (c) open water. The distributions are derived from observed particle fluxes and modeled the deposition velocities, shown separately for periods without potential blowing snow (red) and with potential blowing snow (blue), depending on the blowing snow threshold. The left y-axis (histograms) shows the number of observations, while the right y-axis shows the cumulative frequency distributions for no potential blowing snow (red line), potential blowing snow (blue line), and all observations (black line).

https://doi.org/10.5194/egusphere-2026-1792
Preprint. Discussion started: 8 May 2026

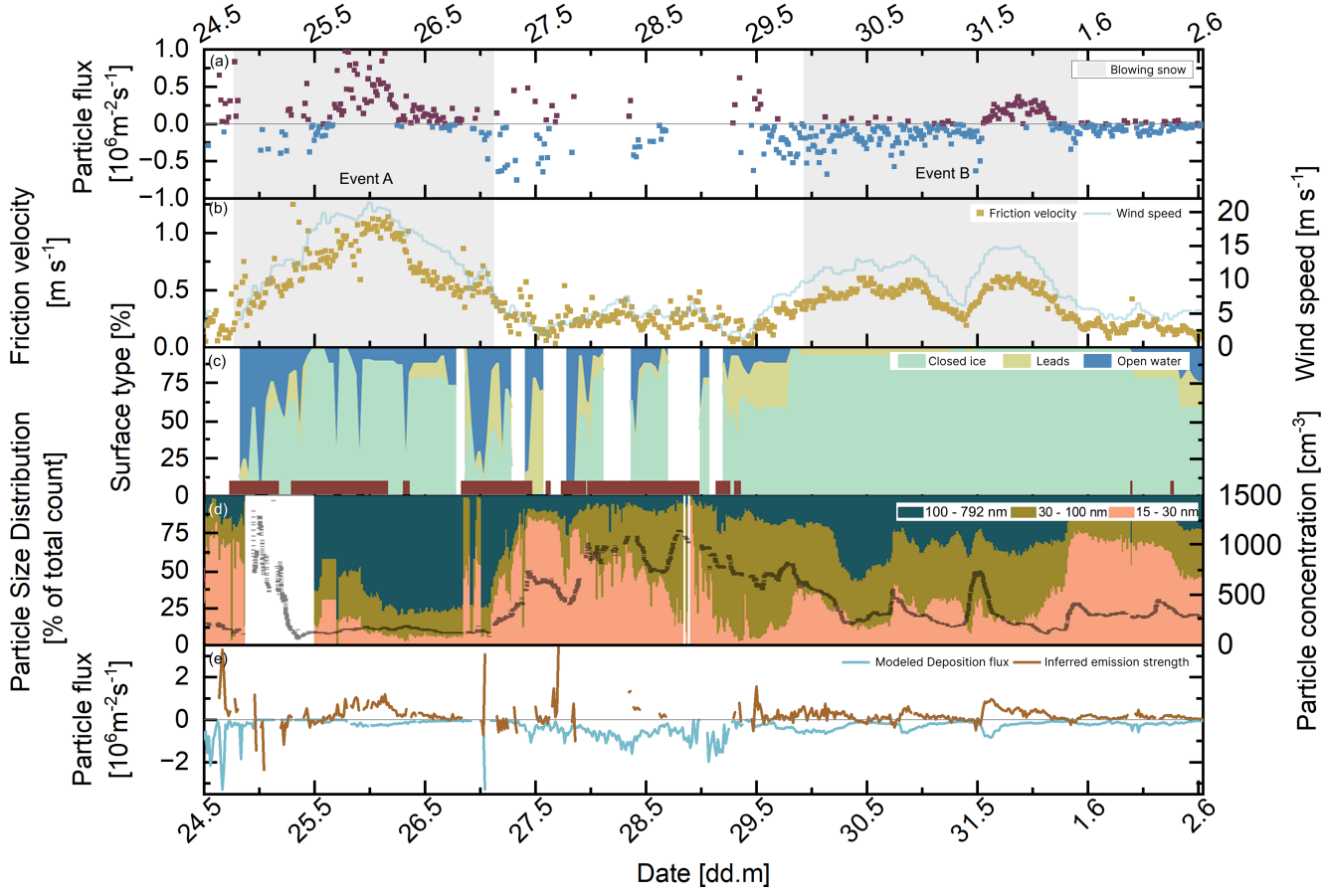

Figure 10. (a) Particle fluxes (in 10^6 m^{-2} s^{-1}) from 24 May to 2 June evaluated in 20-minute intervals, (b) friction velocity (u_*, beige, in m s^{-1}) and wind speed (blue, in m s^{-1}). In (a), the red color indicates net particle emission, and the blue color indicates net particle deposition. The grey shading in (a, b) shows the time periods when the threshold for blowing snow is exceeded. Panel (c) shows the hourly distribution of the three surface types: closed ice (turquoise), leads (beige), and open water (blue). Periods with ship speeds $\geq$ 1 kn are indicated in red. (d) Particle size fractions from 15 to 792 nm in three accumulated groups (left y-axis, in % of total particle number concentration) measured with a DMPS on the fourth deck of *Oden* and total particle number concentration (cm^{-3}), measured with an MCPC at the foremast (black symbols; right y-axis). (e) Modeled deposition flux (turquoise) and inferred emission strength (brown).

3.4 Net particle emission during high wind speed events

In total, eight periods of high wind speed with a potential for blowing snow were identified during the campaign (see Sect. 3.1). Due to the faster mobilization of cold, dry snow, the blowing snow threshold would at times already be reached at wind speeds above 6 m s^{-1} at low temperatures (Fig. A2). Five of these events are characterized by net particle emission. One shows flux values close to zero, and two are dominated by net deposition. Most of the periods of high wind speed occurred when the

https://doi.org/10.5194/egusphere-2026-1792
Preprint. Discussion started: 8 May 2026

prevailing surface type was closed ice. Across all eight events, the median friction velocity ranged from 0.45 to 0.69 m s^{-1}, reflecting consistently enhanced turbulence during conditions favorable for blowing snow. Two emission dominated events, on 24–26 and 29–31 May, are highlighted in Fig 10 as they exhibit strong and persistent particle emission fluxes. Event A (24–26 May) is characterized by strong net emission fluxes of up to $0.98 \times 10^6 \mathrm{m}^{-2}\mathrm{s}^{-1}$ and by being the longest continuous net emission period of the entire measurement campaign (Fig. 10a). The inferred emission strength reached a maximum value of $1.2 \times 10^6 \mathrm{m}^{-2}\mathrm{s}^{-1}$. Figure 10b further shows that the strongest emission fluxes occur nearly simultaneously with peaks in friction velocity and wind speed. During this event, closed ice dominated the surface conditions (Fig. 10c), although individual hours were intermittently influenced by open water. Similarly, during the event from 29 to 31 May (Event B), closed ice remained the predominant surface type, and the inferred emission strength reached values up to $1.57 \times 10^6 \mathrm{m}^{-2}\mathrm{s}^{-1}$ (Fig. 10e). The coincidence of favorable conditions for blowing snow, enhanced turbulence, and net particle emission over predominantly closed ice suggests the presence of a wind related particle source. This is consistent with processes associated with blowing snow, which can temporarily outweigh the deposition fluxes typically observed over closed ice.

One type of particles near the ground that is associated with high wind speeds above sea ice are sea salt aerosols (SSAs), which are produced by the sublimation of blowing snow (Frey et al., 2020). While the open ocean is the largest source of SSA, with wave breaking and bubble bursting generating film and jet drops (e.g., de Leeuw et al., 2011), several studies show that strong SSA sources are also associated with sea ice. Sublimation caused by salty blowing snow is considered a major source of SSA in sea ice dominated environments (Frey et al., 2020; Ranjithkumar et al., 2025). In addition to particles measured in coarse mode (Yang et al., 2019; Ranjithkumar et al., 2025; Frey et al., 2020), Gong et al. (2023) observed an increase in particles ranging from 10 to 300 nm during blowing snow events. The evolution of the particle size distribution in Fig. 10d shows that particles between 100 and 300 nm were dominant during Event A. During Event B, smaller particles were also present. This is consistent with elevated particle concentrations below 300 nm as observed by Gong et al. (2023). Therefore, one possible explanation for the observed net particle emissions during Events A and B is that particles were generated by the sublimation of blowing snow during the high wind speed events. This production outweighs the deposition processes occurring simultaneously on closed ice surfaces. This is also evident in the results of the deposition model (Fig. 10e), which shows an increased inferred emission strength. Furthermore, it becomes clear from Figure 10e that at the onset of Event B, the particle emissions caused by blowing snow are masked by deposition fluxes, so that there is no net emission but deposition at the beginning of this event. Measurements of particle fluxes taken on the ice during the same campaign using the gradient method also indicate emission fluxes associated with blowing snow (Mathes et al., 2025).

Previous modeling studies have often assumed that blowing snow particles consist solely of sea salt (Chen et al., 2022). However, this assumption ignores the chemical complexity of Arctic snow, which has been shown to contain organic matter, as well as nitrate and sulphate (Macdonald et al., 2018; Mori et al., 2019; Grannas et al., 2007). Studies demonstrate that blowing snow events are associated with increased sulfate concentrations (Gong et al., 2023) as well as elevated submicron sodium and chloride masses (Chen et al., 2022). Observations from the ARTofMELT campaign further demonstrate that Arctic snow

https://doi.org/10.5194/egusphere-2026-1792
Preprint. Discussion started: 8 May 2026

contains amounts of organic and biological material as well as black carbon. They highlight that blowing snow particles cannot be assumed to consist of sea salt alone (Pereira Freitas et al., 2025).

3.5 Climatological implications

Using a simple, area-weighted approach based on monthly sea ice extent (Fetterer et al., 2025) and the particle flux measurements taken in this study, it is estimated that the high Arctic Ocean acts as a sink for particles throughout the year. The fractions of the surface covered by ice and open water were determined for each month. The total net particle flux was calculated from the median emission flux over open water and the median deposition flux over closed ice, weighted by their respective fractions. Based on these simplified estimates, the high Arctic Ocean acts as a weak sink during winter and spring (e.g., March 2024 = $-0.02 \times 10^6 \mathrm{m}^{-2}\mathrm{s}^{-1}$) and becomes an even weaker sink during summer and early autumn (e.g., September 2024 = $-0.01 \times 10^6 \mathrm{m}^{-2}\mathrm{s}^{-1}$). On an annual scale, the total net particle flux in 2024 was $-0.02 \times 10^6 \mathrm{m}^{-2}\mathrm{s}^{-1}$. Based on sea ice extent projections under the SSP5-CMIP6 scenario (Deutsches Klimarechenzentrum, 2023), the projected particle sink is expected to be around 5% lower in March and 12% lower in September in the year 2040 compared to 2024. This reflects more open water areas acting as potential particle sources in summer and an Arctic that remains ice-dominated in late winter. In line with broader CMIP6 projections, sea ice loss is expected to continue across all emission scenarios. Several models simulate conditions with almost no sea ice in September by the 2030s, while the average of the models predicts that this threshold will be reached around the middle of the century (Heuzé and Jahn, 2024; Diebold et al., 2023). Consequently, as open water fractions expand and seasonal ice retreat intensifies, the high Arctic is expected to act as a weaker sink for particles. With a projected increase in the frequency and intensity of extreme weather events, such as storms, particle emissions from the surface are likely to increase. This may lead to periods when the region acts as a net particle source. At the same time, particle concentrations in the Arctic vary considerably throughout the year. Therefore, the fraction of open water alone is not the only controlling factor.

4 Summary and conclusions

During the ARTofMELT campaign, turbulent particle fluxes in the high Arctic were successfully determined using a continuous five week eddy covariance dataset. The measurements were conducted under a variety of meteorological and surface conditions. The results provide insight into the spatial and temporal variability of particle exchange processes over different surface types, such as closed ice, leads, and open water, in a region undergoing rapid climate change.

Throughout the campaign, periods of net particle emission and periods of net particle deposition were observed, with deposition slightly predominating (58% of all 20-minute flux intervals). Median net deposition fluxes of $-0.02 \times 10^6 \mathrm{m}^{-2}\mathrm{s}^{-1}$ over closed ice confirm that this surface type generally acts as a particle sink under low to moderately turbulent conditions. However, net particle emission fluxes over closed ice were observed during periods of strong winds and increased turbulence with friction velocities $u_* > 0.45$ m s^{-1}. Under such conditions, the mobilization and sublimation of blowing snow might act as a source of particles in the atmosphere. The resulting net emission fluxes reached $0.98 \times 10^6\,\mathrm{m}^{-2}\,\mathrm{s}^{-1}$, much higher than

https://doi.org/10.5194/egusphere-2026-1792
Preprint. Discussion started: 8 May 2026

the deposition fluxes. These strong particle emission events were accompanied by an increase in total particle concentration, suggesting that particle emissions from blowing snow can temporarily dominate the local aerosol budget and mask the deposition typically observed over ice surfaces. This interpretation is supported by the comparison of measured net particle fluxes with modeled deposition fluxes, which reveals enhanced inferred emission during high wind speed events over closed ice. Net particle emission was also observed during periods influenced by open water. However, the magnitude and variability of these fluxes suggest that the role of open water is ambiguous. Leads exhibited deposition and emission events, with median fluxes close to zero. This reflects their dual role as both a particle source and a particle sink.

Our results demonstrate that surface heterogeneity has a strong influence on turbulent particle fluxes in the high Arctic. The emission fluxes observed in this study, and their contribution to local particle concentrations, suggest that particle emissions from leads could impact the microphysics of Arctic clouds under suitable meteorological conditions. However, this influence has yet to be quantified. Climate models predict continued sea ice loss and a corresponding increase in open water areas (IPCC, 2023). Changes in the frequency and intensity of particle exchange processes associated with sea ice are expected. Such changes may influence the background aerosol population and thereby affect concentrations of particles relevant to cloud formation and cloud properties. However, the net effect remains poorly constrained and depends on competing source and sink processes.

The overall climatic effects of changing particle and CCN number concentrations in the Arctic, whether cooling due to increased cloud albedo or warming due to changes in cloud lifetime and phase, remain uncertain (e.g., Cox et al., 2015; Schmale et al., 2021; Tan et al., 2023). In summary, this study has improved our understanding of the interactions between particles, surfaces, and the atmosphere in the Arctic. The quantitative characterization of particle deposition on closed ice and particle emissions from leads can help to better constrain and reduce uncertainties in model simulations of Arctic aerosol-cloud-climate interactions.

Data availability. The dataset is being uploaded to Pangaea.

https://doi.org/10.5194/egusphere-2026-1792
Preprint. Discussion started: 8 May 2026

Appendix A

A1

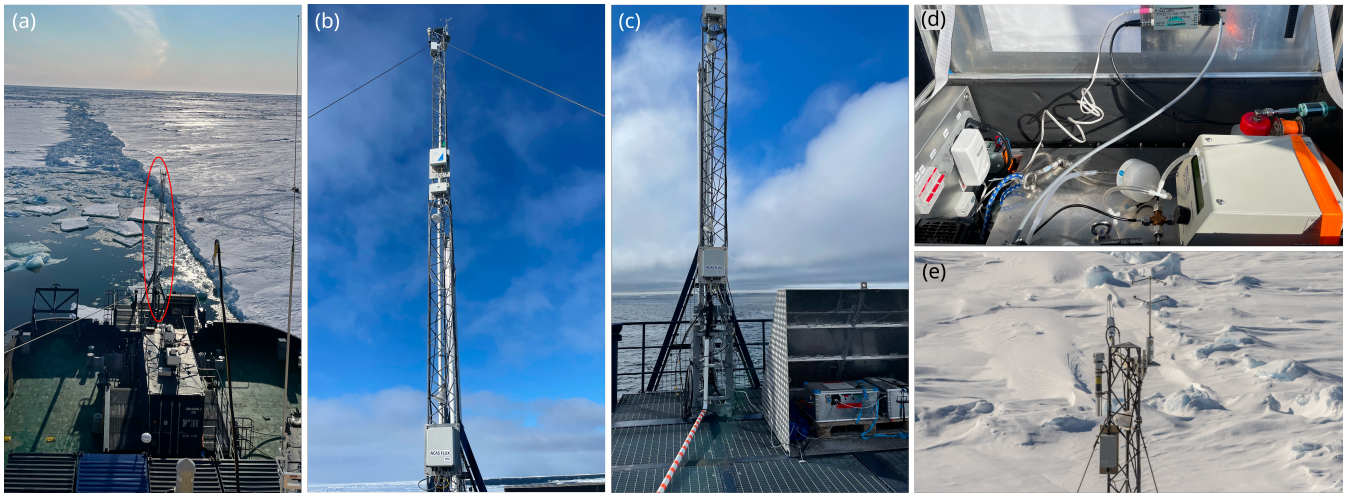

Figure A1. Pictures of the eddy covariance instrumentation installed on the foremast of *Oden*. (a) Forward looking view of the foredeck illustrating the position of the foremast at the bow of the ship (the red circle shows the foremast). (b) View of the foremast showing the sonic anemometer mounted at the top of the mast. (c) View of the lower part of the foremast with the aluminium housing containing the MCPC installed at the base of the mast. (d) MCPC with bypass system in the aluminium housing. (e) View of the top of the foremast with the sonic anemometer (Image credit M.Tjernström).

https://doi.org/10.5194/egusphere-2026-1792
Preprint. Discussion started: 8 May 2026

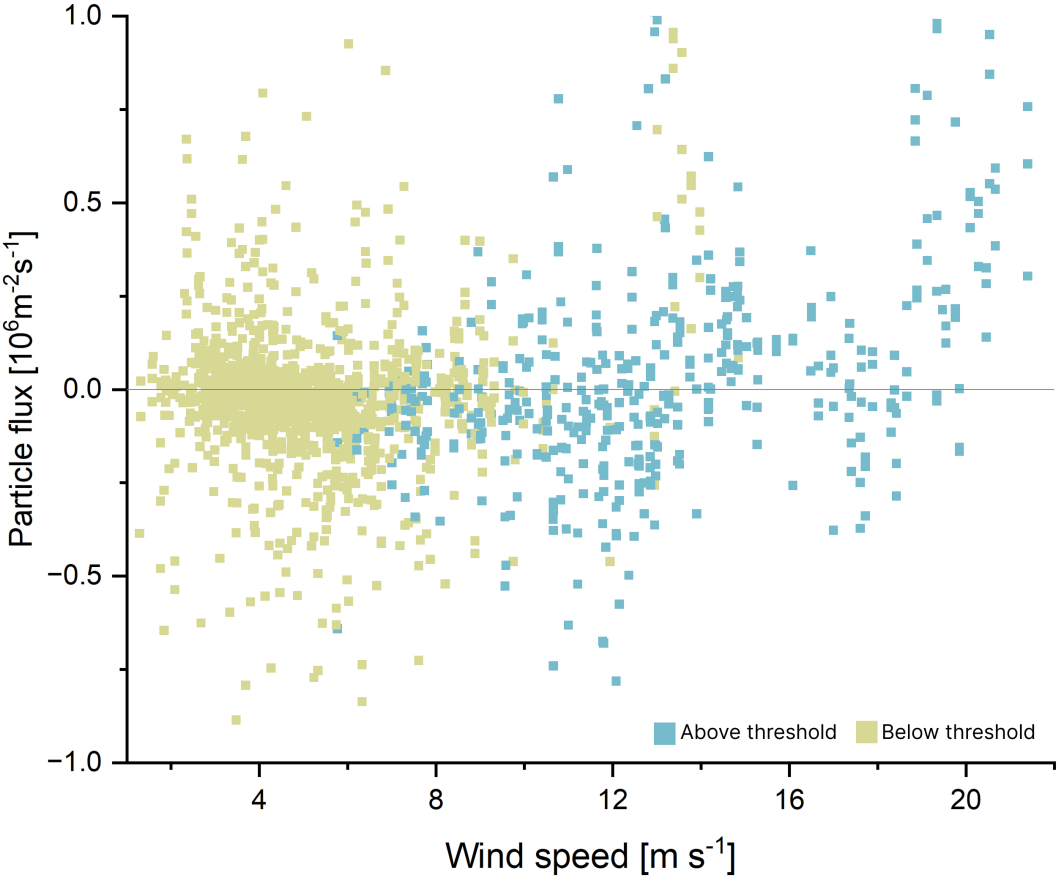

Figure A2. Net particle flux (in 10^6 m^{-2} s^{-1}) for closed ice as a function of wind speed (in m s^{-1}). Colors indicate whether the blowing snow threshold is exceeded (beige: below threshold, turquoise: above threshold), highlighting the conditions under which snow transport is initiated.

https://doi.org/10.5194/egusphere-2026-1792
Preprint. Discussion started: 8 May 2026

Table A1. Parameters and constants used for the calculation of size-resolved dry deposition velocities following Zhang et al. (2001), with modifications after Emerson et al. (2020).

Parameter	Value / Source	Description / Source
z	20.3 m	Measurement height
z_0	0.0002 m	Aerodynamic roughness length (Nilsson and Rannik, 2001; Held et al., 2011a)
κ	0.4	von Kármán constant
g	9.81 m s^{-2}	Gravitational acceleration
p	1013.25 Pa	Ambient air pressure (assumed constant)
ρ_p	1769 kg m^{-3}	Particle density (sea-salt dominated aerosol)
T	measured	Ambient air temperature (K)
u_*	measured	Friction velocity (m s^{-1})
z/L	measured	Stability parameter (Monin Obukhov similarity theory)
$\mu(T)$	Sutherland´s law	Dynamic viscosity of air
$\rho_{\text{air}}(T,p)$	ideal gas law	Air density
$\lambda(T,p)$	temperature pressure dependent	Mean free path of air
$C_c(D_p)$	Cunningham	Slip correction factor
D_p	15–792 nm	Particle diameter (DMPS bins)
$D(D_p)$	calculated	Brownian diffusivity
Sc	calculated	Schmidt number
$v_g(D_p)$	calculated	Gravitational settling velocity
$\phi_H(z/L)$	Businger–Dyer	Stability correction for heat
R_a	calculated	Aerodynamic resistance
R_s	calculated	Surface resistance
e_0	3.0	Empirical constant for smooth surfaces (Zhang et al. 2001)
γ	2/3	Brownian diffusion exponent (Emerson et al. 2018)
C_B	0.2	Brownian collection efficiency coefficient (Emerson et al. 2018)
A	0.01 m	Collector radius (interception scale)
E_{IN}	0	Interception efficiency (neglected for smooth ice/water)
$v_d(D_p)$	calculated	Modeled dry deposition velocity

Author contributions. TM: conceptualization, methodology, measurements, data analysis and writing. Review and editing, with conceptual contributions from IB, SM, MT, JK, PZ, JP, BW and AH. IB provided the surface images. SM and JP provided the motion corrected sonic data, meteorological data, as well as the sensible heat flux data. JK and PZ measured and provided the particle size distribution data. Supervision: AH.

https://doi.org/10.5194/egusphere-2026-1792
Preprint. Discussion started: 8 May 2026

Competing interests. At least one of the (co-)authors is a member of the editorial board of Atmospheric Chemistry and Physics.

Acknowledgements. This work is part of the ARTofMELT (Atmospheric rivers and the onset of Arctic melt) project. The ARTofMELT expedition was supported and organized by the Swedish Polar Research Secretariat (SPRS) on the Swedish research icebreaker *Oden* in spring 2023 under the SWEDARCTIC program. Support also came from the Swedish Council for Research Infrastructures (Grant 2021-00153) and the Knut and Alice Wallenberg Foundation (Grant 2016-0024) as well as from the Natural Environment Research Council UK (Grant NE/X000087/1 and Grant RG/EVEA/125876/001). This study was funded by the Deutsche Forschungsgemeinschaft (DFG, German Research Foundation) – HE5214/10-1, HE5214/11-1 and WE2757/6-1. This work also received support from the European Union's Horizon 2020 research and innovation programme under grant agreement 101003826 via project CRiceS (Climate Relevant interactions and feedbacks: the key role of sea ice and Snow in the polar and global climate system) and the European Research Council (Consolidator grant INTEGRATE 865799). Additional funding was provided by the European Union's Horizon Europe project "CleanCloud" (Grant agreement 101137639) as well as by the Carl Tryggers Foundation (CTS 22:2148), Ymer-80-foundation, the Bolin Centre for Climate Research (RA2) and the Ivar Bendixsons scholarship.

The authors are grateful to the co-Chief Scientists Michael Tjernström and Paul Zieger, the SPRS coordinator Åsa Lindgren and the SPRS support team, and to Captain Mattias Petersson and the crew on *Oden*. The authors would like to thank Max Zeidler, Andre Backhoff and Sven Klemer for technical support. We thank Philipp Oehlke for his support during the assembly of the MCPC measurement box. We would like to thank the students at the Institute for Environmental Technology at TU Berlin for their invaluable help with image analysis. We would also like to thank XX and XX for their helpful comments as reviewers. I acknowledge the use of *DeepL Write* and *Grammarly* for the preparation of the manuscript.

https://doi.org/10.5194/egusphere-2026-1792
Preprint. Discussion started: 8 May 2026

References

Albrecht, B. A.: Aerosols, cloud microphysics, and fractional cloudiness, Science (New York, N.Y.), 245, 1227–1230, https://doi.org/10.1126/science.245.4923.1227, 1989.

Andreas, E. L., Persson, P. O. G., Grachev, A. A., Jordan, R. E., Horst, T. W., Guest, P. S., and Fairall, C. W.: Parameterizing Turbulent Exchange over Sea Ice in Winter, Journal of Hydrometeorology, 11, 87–104, https://doi.org/10.1175/2009JHM1102.1, 2010.

Anguelova, M. and Huq, P.: Characteristics of bubble clouds at various wind speeds, Journal of Geophysical Research, 117, 1–22, https://doi.org/10.1029/2011JC007442, 2012.

Arctic Monitoring and Assessment Programme, ed.: AMAP Assessment 2021: Impacts of Short-lived Climate Forcers on Arctic Climate, Air Quality, and Human Health., AMAP, Tromsø, Norway, 2021.

Baccarini, A., Karlsson, L., Dommen, J., Duplessis, P., Vüllers, J., Brooks, I. M., Saiz-Lopez, A., Salter, M., Tjernström, M., Baltensperger, U., Zieger, P., and Schmale, J.: Frequent new particle formation over the high Arctic pack ice by enhanced iodine emissions, Nature Communications, 11, https://doi.org/10.1038/s41467-020-18551-0, 2020.

Beck, I., Angot, H., Baccarini, A., Dada, L., Quéléver, L., Jokinen, T., Laurila, T., Lampimäki, M., Bukowiecki, N., Boyer, M., Gong, X., Gysel-Beer, M., Petäjä, T., Wang, J., and Schmale, J.: Automated identification of local contamination in remote atmospheric composition time series, Atmospheric Measurement Techniques, 15, 4195–4224, https://doi.org/10.5194/amt-15-4195-2022, 2022.

Bullard, J. E., Baddock, M., Bradwell, T., Crusius, J., Darlington, E., Gaiero, D., Gassó, S., Gisladottir, G., Hodgkins, R., McCulloch, R., McKenna-Neuman, C., Mockford, T., Stewart, H., and Thorsteinsson, T.: High-latitude dust in the Earth system, Reviews of Geophysics, 54, 447–485, https://doi.org/10.1002/2016RG000518, 2016.

Carslaw, K., Lee, L., Reddington, C., Pringle, K., Rap, A., Forster, P., Mann, G., Spracklen, D., Woodhouse, M., Regayre, L., and Pierce, J.: Large contribution of natural aerosols to uncertainty in indirect forcing, Nature, 503, 67–71, https://doi.org/10.1038/nature12674, 2013.

Chen, Q., Mirrielees, J. A., Thanekar, S., Loeb, N. A., Kirpes, R. M., Upchurch, L. M., Barget, A. J., Lata, N. N., Raso, A. R. W., McNamara, S. M., China, S., Quinn, P. K., Ault, A. P., Kennedy, A., Shepson, P. B., Fuentes, J. D., and Pratt, K. A.: Atmospheric particle abundance and sea salt aerosol observations in the springtime Arctic: a focus on blowing snow and leads, Atmospheric Chemistry and Physics, 22, 15 263–15 285, https://doi.org/10.5194/acp-22-15263-2022, 2022.

Chylek, P., Vogelsang, T. J., Klett, J. D., Hengartner, N., Higdon, D., Lesins, G., and Dubey, M. K.: Indirect Aerosol Effect Increases CMIP5 Models' Projected Arctic Warming, Journal of Climate, 29, 1417–1428, https://doi.org/10.1175/JCLI-D-15-0362.1, 2016.

Cohen, J., Screen, J. A., Furtado, J. C., Barlow, M., Whittleston, D., Coumou, D., Francis, J., Dethloff, K., Entekhabi, D., Overland, J., and Jones, J.: Recent Arctic amplification and extreme mid-latitude weather, Nature Geoscience, 7, 627–637, https://doi.org/10.1038/ngeo2234, 2014.

Contini, D., Donateo, A., Belosi, F., Grasso, F. M., Santachiara, G., and Prodi, F.: Deposition velocity of ultrafine particles measured with the Eddy–Correlation Method over the Nansen Ice Sheet (Antarctica), Journal of Geophysical Research: Oceans, 115, https://doi.org/10.1029/2009JD013600, 2010.

Cox, C. J., Walden, V. P., Rowe, P. M., and Shupe, M. D.: Humidity trends imply increased sensitivity to clouds in a warming Arctic, Nature Communications, 6, https://doi.org/10.1038/ncomms10117, 2015.

Creamean, J. M., Barry, K., Hill, T. C. J., Hume, C., DeMott, P. J., Shupe, M. D., Dahlke, S., Willmes, S., Schmale, J., Beck, I., Hoppe, C. J. M., Fong, A., Chamberlain, E., Bowman, J., Scharien, R., and Persson, O.: Annual cycle observations of aerosols capable of ice formation in central Arctic clouds, Nature Communications, 13, 3537, https://doi.org/10.1038/s41467-022-31182-x, 2022.

https://doi.org/10.5194/egusphere-2026-1792
Preprint. Discussion started: 8 May 2026

de Leeuw, G., Andreas, E. L., Anguelova, M. D., Fairall, C. W., Lewis, E. R., O'Dowd, C., Schulz, M., and Schwartz, S. E.: Production flux of sea spray aerosol, Reviews of Geophysics, 49, https://doi.org/10.1029/2010RG000349, 2011.

Deutsches Klimarechenzentrum: CMIP6 Climate Simulations: Sea Ice, https://www.dkrz.de/en/communication/climate-simulations/cmip6-en/results/sea-ice, accessed: 2025-11-13, 2023.

Diebold, F. X., Rudebusch, G. D., Göbel, M., Goulet Coulombe, P., and Zhang, B.: When will Arctic sea ice disappear? Projections of area, extent, thickness, and volume, Journal of Econometrics, 236, 105 479, https://doi.org/10.1016/j.jeconom.2023.105479, 2023.

Donateo, A. and Contini, D.: Correlation of Dry Deposition Velocity and Friction Velocity over Different Surfaces for PM2.5 and Particle Number Concentrations, Advances in Meteorology, 2014, https://doi.org/10.1155/2014/760393, 2014.

Donateo, A., Pappaccogli, G., Famulari, D., Mazzola, M., Scoto, F., and Decesari, S.: Characterization of size-segregated particles' turbulent flux and deposition velocity by eddy correlation method at an Arctic site, Atmos. Chem. Phys., 23, 7425–7445, https://doi.org/10.5194/acp-23-7425-2023, 2023.

Donateo, A., Pappaccogli, G., Scoto, F., Busetto, M., Lovisco, F. L., Brett, N., Keller, D., Barret, B., Dieudonné, E., Pohorsky, R., Baccarini, A., Bekki, S., Raut, J.-C., Schmale, J., Law, K. S., Arnold, S. R., Fochesatto, G. J., Simpson, W. R., and Decesari, S.: Aerosol dry deposition fluxes on snow during the ALPACA campaign in Fairbanks, Alaska, https://doi.org/10.5194/egusphere-2025-1366, 2025.

Edson, J. B., Hinton, A. A., Prada, K. E., Hare, J. E., and Fairall, C. W.: Direct Covariance Flux Estimates from Mobile Platforms at Sea*, Journal of Atmospheric and Oceanic Technology, 15, 547–562, https://doi.org/10.1175/1520-0426(1998)015<0547:DCFEFM>2.0.CO;2, 1998.

Emerson, E. W., Hodshire, A. L., DeBolt, H. M., Bilsback, K. R., Pierce, J. R., McMeeking, G. R., and Farmer, D. K.: Revisiting particle dry deposition and its role in radiative effect estimates, Proceedings of the National Academy of Sciences of the United States of America, 117, 26 076–26 082, https://doi.org/10.1073/pnas.2014761117, 2020.

Farmer, D. K., Boedicker, E. K., and DeBolt, H. M.: Dry Deposition of Atmospheric Aerosols: Approaches, Observations, and Mechanisms, Annual review of physical chemistry, 72, 375–397, https://doi.org/10.1146/annurev-physchem-090519-034936, 2021.

Farmer, D. M., McNeil, C. L., and Johnson, B. D.: Evidence for the importance of bubbles in increasing air–sea gas flux, Nature, 361, 620–623, https://doi.org/10.1038/361620a0, 1993.

Fetterer, F., Knowles, K., Meier, W. N., Savoie, M., Windnagel, A., and Stafford, T.: Sea Ice Index, Version 4, https://doi.org/10.7265/A98X-0F50, 2025.

Foken, T. and Mauder, M.: Micrometeorology, Springer Atmospheric Sciences, Springer International Publishing, Cham, ISBN 978-3-031-47525-2 978-3-031-47526-9, https://doi.org/10.1007/978-3-031-47526-9, 2024.

Frey, M. M., Norris, S. J., Brooks, I. M., Anderson, P. S., Nishimura, K., Yang, X., Jones, A. E., Nerentorp Mastromonaco, M. G., Jones, D. H., and Wolff, E. W.: First direct observation of sea salt aerosol production from blowing snow above sea ice, Atmospheric Chemistry and Physics, 20, 2549–2578, https://doi.org/10.5194/acp-20-2549-2020, 2020.

Garrett, T. J., Zhao, C., and Novelli, P. C.: Assessing the relative contributions of transport efficiency and scavenging to seasonal variability in Arctic aerosol, Tellus B: Chemical and Physical Meteorology, 62, 190, https://doi.org/10.1111/j.1600-0889.2010.00453.x, 2010.

Gong, X., Zhang, J., Croft, B., Yang, X., Frey, M. M., Bergner, N., Chang, R. Y.-W., Creamean, J. M., Kuang, C., Martin, R. V., Ranjithkumar, A., Sedlacek, A. J., Uin, J., Willmes, S., Zawadowicz, M. A., Pierce, J. R., Shupe, M. D., Schmale, J., and Wang, J.: Arctic warming by abundant fine sea salt aerosols from blowing snow, Nature geoscience, 16, 768–774, https://doi.org/10.1038/s41561-023-01254-8, 2023.

Gormley, P. G. and Kennedy, M.: Diffusion from a Stream Flowing through a Cylindrical Tube, Proc. Royal Irish Academy, pp. 163–169, 1949.

https://doi.org/10.5194/egusphere-2026-1792
Preprint. Discussion started: 8 May 2026

Grachev, A. A., Fairall, C. W., Persson, P. O. G., Andreas, E. L., and Guest, P. S.: Stable Boundary-Layer Scaling Regimes: The Sheba Data, Boundary-Layer Meteorology, 116, 201–235, https://doi.org/10.1007/s10546-004-2729-0, 2005.

Grannas, A. M., Jones, A. E., Dibb, J., Ammann, M., Anastasio, C., Beine, H. J., Bergin, M., Bottenheim, J., Boxe, C. S., Carver, G., Chen, G., Crawford, J. H., Dominé, F., Frey, M. M., Guzmán, M. I., Heard, D. E., Helmig, D., Hoffmann, M. R., Honrath, R. E., Huey, L. G., Hutterli, M., Jacobi, H. W., Klán, P., Lefer, B., McConnell, J., Plane, J., Sander, R., Savarino, J., Shepson, P. B., Simpson, W. R., Sodeau, J. R., von Glasow, R., Weller, R., Wolff, E. W., and Zhu, T.: An overview of snow photochemistry: evidence, mechanisms and impacts, Atmospheric Chemistry and Physics, 7, 4329–4373, https://doi.org/10.5194/acp-7-4329-2007, 2007.

Grönlund, A., Nilsson, D., Koponen, I. K., Virkkula, A., and Hansson, M. E.: Aerosol dry deposition measured with eddy-covariance technique at Wasa and Aboa, DronningMaud Land, Antarctica, Annals of Glaciology, 35, 355–361, https://doi.org/10.3189/172756402781816519, 2002.

Grönholm, T., Launiainen, S., Ahlm, L., Mårtensson, E. M., Kulmala, M., Vesala, T., and Nilsson, E. D.: Aerosol particle dry deposition to canopy and forest floor measured by two-layer eddy covariance system, Journal of Geophysical Research: Atmospheres, 114, https://doi.org/10.1029/2008JD010663, 2009.

Heintzenberg, J., Leck, C., and Tunved, P.: Potential source regions and processes of aerosol in the summer Arctic, Atmospheric Chemistry and Physics, 15, 6487–6502, https://doi.org/10.5194/acp-15-6487-2015, 2015.

Held, A., Brooks, I. M., Leck, C., and Tjernström, M.: On the potential contribution of open lead particle emissions to the central Arctic aerosol concentration, Atmos. Chem. Phys., 11, 3093–3105, https://doi.org/10.5194/acp-11-3093-2011, 2011a.

Held, A., Orsini, D. A., Vaattovaara, P., Tjernström, M., and Leck, C.: Near-surface profiles of aerosol number concentration and temperature over the Arctic Ocean, Atmospheric Measurement Techniques, 4, 1603–1616, https://doi.org/10.5194/amt-4-1603-2011, 2011b.

Heutte, B., Bergner, N., Angot, H., Pernov, J. B., Dada, L., Mirrielees, J. A., Beck, I., Baccarini, A., Boyer, M., Creamean, J. M., Daellenbach, K. R., El Haddad, I., Frey, M. M., Henning, S., Laurila, T., Moschos, V., Petäjä, T., Pratt, K. A., Quéléver, L. L. J., Shupe, M. D., Zieger, P., Jokinen, T., and Schmale, J.: Observations of high-time-resolution and size-resolved aerosol chemical composition and microphysics in the central Arctic: implications for climate-relevant particle properties, Atmospheric Chemistry and Physics, 25, 2207–2241, https://doi.org/10.5194/acp-25-2207-2025, 2025.

Heuzé, C. and Jahn, A.: The first ice-free day in the Arctic Ocean could occur before 2030, Nature Communications, 15, 10 101, https://doi.org/10.1038/s41467-024-54508-3, 2024.

Horst, T. W.: A simple formula for attenuation of eddy fluxes measured with first-order-response scalar sensors, Boundary-Layer Meteorology, 82, 219–233, https://doi.org/10.1023/A:1000229130034, 1997.

IPCC: Summary for Policymakers. In: *Climate Change 2023: Synthesis Report. Contribution of Working Groups I, II and III to the Sixth Assessment Report of the Intergovernmental Panel on Climate Change* [Core Writing Team, H. Lee and J. Romero (eds.)], Tech. rep., Intergovernmental Panel on Climate Change (IPCC), Geneva, Switzerland, https://doi.org/10.59327/IPCC/AR6-9789291691647.001, 2023.

Johnson, B. D. and Wangersky, P. J.: Microbubbles: Stabilization by monolayers of adsorbed particles, Journal of Geophysical Research: Oceans, 92, 14 641–14 647, https://doi.org/10.1029/JC092iC13p14641, 1987.

Kanji, Z. A., Ladino, L. A., Wex, H., Boose, Y., Burkert-Kohn, M., Cziczo, D. J., and Krämer, M.: Overview of Ice Nucleating Particles, Meteorological Monographs, 58, 1.1–1.33, https://doi.org/10.1175/AMSMONOGRAPHS-D-16-0006.1, 2017.

Karlsson, L., Baccarini, A., Duplessis, P., Baumgardner, D., Brooks, I. M., Chang, R. Y.-W., Dada, L., Dällenbach, K. R., Heikkinen, L., Krejci, R., Leaitch, W. R., Leck, C., Partridge, D. G., Salter, M. E., Wernli, H., Wheeler, M. J., Schmale, J., and Zieger, P.: Physical and

https://doi.org/10.5194/egusphere-2026-1792
Preprint. Discussion started: 8 May 2026

Chemical Properties of Cloud Droplet Residuals and Aerosol Particles During the Arctic Ocean 2018 Expedition, Journal of Geophysical Research: Atmospheres, 127, e2021JD036 383, https://doi.org/10.1029/2021JD036383, 2022.

Kirpes, R. M., Bonanno, D., May, N. W., Fraund, M., Barget, A. J., Moffet, R. C., Ault, A. P., and Pratt, K. A.: Wintertime Arctic Sea Spray Aerosol Composition Controlled by Sea Ice Lead Microbiology, ACS Central Science, 5, 1760–1767, https://doi.org/10.1021/acscentsci.9b00541, 2019.

Koike, M., Takigawa, M., Morimoto, S., Adachi, K., Aizawa, T., Chandra, N., Fujita, R., Goto, D., Ishidoya, S., Ishijima, K., Ito, A., Kawai, K., Kanaya, Y., Kim, Y., Kinase, T., Kondo, Y., Machida, T., Matsui, H., Miyakawa, T., Mochida, M., Mori, T., Moteki, N., Murayama, S., Ohata, S., Oshima, N., Patra, P. K., Taketani, F., Tobo, Y., Tohjima, Y., Toyoda, S., Tsuboi, K., Rui, O. C., Yahara, K., Yamaji, K., Yoshida, A., and Zhu, C.: Studies of atmospheric climate forcers in the Arctic during the ArCS II project, Polar Science, https://doi.org/10.1016/j.polar.2025.101216, 2025.

Korhonen, H., Carslaw, K., Spracklen, D., Ridley, D., and Ström, J.: A global model study of processes controlling aerosol size distributions in the Arctic spring and summer, Journal of Geophysical Research, 113, https://doi.org/10.1029/2007JD009114, 2008.

Kulkarni, P., Baron, P. A., and Willeke, K., eds.: Aerosol Measurement: Principles, Techniques, and Applications, Wiley, J, New York, NY, 3., auflage edn., ISBN 9780470387412, 2011.

Kulmala, M., Vehkamäki, H., Petäjä, T., Dal Maso, M., Lauri, A., Kerminen, V. M., Birmili, W., and McMurry, P. H.: Formation and growth rates of ultrafine atmospheric particles: a review of observations, Journal of Aerosol Science, 35, 143–176, https://doi.org/10.1016/j.jaerosci.2003.10.003, 2004.

Lapere, R., Thomas, J. L., Marelle, L., Ekman, A. M. L., Frey, M. M., Lund, M. T., Makkonen, R., Ranjithkumar, A., Salter, M. E., Samset, B. H., Schulz, M., Sogacheva, L., Yang, X., and Zieger, P.: The Representation of Sea Salt Aerosols and Their Role in Polar Climate Within CMIP6, Journal of Geophysical Research: Atmospheres, 128, https://doi.org/10.1029/2022JD038235, 2023.

Lapere, R., Marelle, L., Rampal, P., Brodeau, L., Melsheimer, C., Spreen, G., and Thomas, J. L.: Modeling the contribution of leads to sea spray aerosol in the high Arctic, Atmos. Chem. Phys., https://doi.org/https://doi.org/10.5194/acp-24-12107-2024, 2024.

Law, K. S. and Stohl, A.: Arctic Air Pollution: Origins and Impacts, Science, 315, 1537–1540, https://doi.org/10.1126/science.1137695, 2007.

Leck, C., Norman, M., Bigg, E. K., and Hillamo, R.: Chemical composition and sources of the high Arctic aerosol relevant for cloud formation, Journal of Geophysical Research: Atmospheres, 107, https://doi.org/10.1029/2001JD001463, 2002.

Li, L. and Pomeroy, J. W.: Probability of occurrence of blowing snow, Journal of Geophysical Research: Atmospheres, 102, 21 955–21 964, https://doi.org/10.1029/97JD01522, 1997.

LI-COR, Inc.: EddyPro Software (Version 7.0) [Computer software], 2021.

Macdonald, K. M., Sharma, S., Toom, D., Chivulescu, A., Platt, A., Elsasser, M., Huang, L., Leaitch, R., Chellman, N., McConnell, J. R., Bozem, H., Kunkel, D., Lei, Y. D., Jeong, C.-H., Abbatt, J. P. D., and Evans, G. J.: Temporally delineated sources of major chemical species in high Arctic snow, Atmospheric Chemistry and Physics, 18, 3485–3503, https://doi.org/10.5194/acp-18-3485-2018, 2018.

Mathes, T., Guy, H., Prytherch, J., Kojoj, J., Brooks, I., Murto, S., Zieger, P., Wehner, B., Tjernström, M., and Held, A.: Particle flux–gradient relationships in the high Arctic: emission and deposition patterns across three surface types, Atmospheric Chemistry and Physics, 25, 8455–8474, https://doi.org/10.5194/acp-25-8455-2025, 2025.

Mauder, M., Cuntz, M., Drüe, C., Graf, A., Rebmann, C., Schmid, H. P., Schmidt, M., and Steinbrecher, R.: A strategy for quality and uncertainty assessment of long-term eddy-covariance measurements, Agricultural and Forest Meteorology, 169, 122–135, https://doi.org/10.1016/j.agrformet.2012.09.006, 2013.

https://doi.org/10.5194/egusphere-2026-1792
Preprint. Discussion started: 8 May 2026

Mauritsen, T., Sedlar, J., Tjernström, M., Leck, C., Martin, M., Shupe, M., Sjogren, S., Sierau, B., Persson, P. O. G., Brooks, I. M., and Swietlicki, E.: An Arctic CCN-limited cloud-aerosol regime, Atmos. Chem. Phys., 11, 165–173, https://doi.org/10.5194/acp-11-165-2011, 2011.

May, N. W., Quinn, P. K., McNamara, S. M., and Pratt, K. A.: Multiyear study of the dependence of sea salt aerosol on wind speed and sea ice conditions in the coastal Arctic, Journal of Geophysical Research: Atmospheres, 121, 9208–9219, https://doi.org/10.1002/2016JD025273, 2016.

Meredith, M., Sommerkorn, M., Cassotta, S., Derksen, C., Ekaykin, A., Hollowed, A., Kofinas, G., Mackintosh, A., Melbourne-Thomas, J., Muelbert, M., Ottersen, G., Pritchard, H., and Schuur, E.: Polar Regions: In: IPCC Special Report on the Ocean and Cryosphere in a Changing Climate, IPCC, https://www.ipcc.ch/site/assets/uploads/sites/3/2019/11/07_SROCC_Ch03_FINAL.pdf, 2019.

Mirrielees, J. A., Kirpes, R. M., Costa, E. J., Porter, G. C. E., Murray, B. J., Lata, N. N., Boschi, V., China, S., Grannas, A. M., Ault, A. P., Matrai, P. A., and Pratt, K. A.: Marine aerosol generation experiments in the High Arctic during summertime, Elementa: Science of the Anthropocene, 12, 00 134, https://doi.org/10.1525/elementa.2023.00134, 2024.

Moat, B. I. and Yelland, M. J.: Airflow distortion at instrument sites on the RRS James Clark Ross during the WAGES project, https://nora.nerc.ac.uk/id/eprint/509304/, 2015.

Mohan, S.: An overview of particulate dry deposition: measuring methods, deposition velocity and controlling factors, International Journal of Environmental Science and Technology, 13, https://doi.org/10.1007/s13762-015-0898-7, 2015.

Moncrieff, J., Clement, R., Finnigan, J., and Meyers, T.: Averaging, Detrending, and Filtering of Eddy Covariance Time Series, in: Handbook of Micrometeorology, edited by Lee, X., Massman, W., and Law, B., vol. 29, pp. 7–31, Kluwer Academic Publishers, Dordrecht, ISBN 978-1-4020-2264-7, https://doi.org/10.1007/1-4020-2265-4_2, 2005.

Moncrieff, J., Clement, R., Finnigan, J., and Meyers, T.: Averaging, Detrending, and Filtering of Eddy Covariance Time Series, in: Handbook of Micrometeorology, Atmospheric and Oceanographic Sciences Library, vol. 29, pp. 7–31, ISBN 978-1-4020-2264-7, https://doi.org/10.1007/1-4020-2265-4_2, 2006.

Mori, T., Goto-Azuma, K., Kondo, Y., Ogawa-Tsukagawa, Y., Miura, K., Hirabayashi, M., Oshima, N., Koike, M., Kupiainen, K., Moteki, N., Ohata, S., Sinha, P., Sugiura, K., Aoki, T., Schneebeli, M., Steffen, K., Sato, A., Tsushima, A., Makarov, V., Omiya, S., Sugimoto, A., Takano, S., and Nagatsuka, N.: Black Carbon and Inorganic Aerosols in Arctic Snowpack, Journal of Geophysical Research: Atmospheres, 124, 13 325–13 356, https://doi.org/10.1029/2019JD030623, 2019.

Moschos, V., Dzepina, K., Bhattu, D., Lamkaddam, H., Casotto, R., Daellenbach, K. R., Canonaco, F., Rai, P., Aas, W., Becagli, S., Calzolai, G., Eleftheriadis, K., Moffett, C. E., Schnelle-Kreis, J., Severi, M., Sharma, S., Skov, H., Vestenius, M., Zhang, W., Hakola, H., Hellén, H., Huang, L., Jaffrezo, J.-L., Massling, A., Nøjgaard, J. K., Petäjä, T., Popovicheva, O., Sheesley, R. J., Traversi, R., Yttri, K. E., Schmale, J., Prévôt, A. S. H., Baltensperger, U., and El Haddad, I.: Equal abundance of summertime natural and wintertime anthropogenic Arctic organic aerosols, Nature Geoscience, 15, 196–202, https://doi.org/10.1038/s41561-021-00891-1, 2022.

Mulhearn, P. J.: Distribution of microbubbles in coastal waters, Journal of Geophysical Research: Oceans, 86, 6429–6434, https://doi.org/10.1029/JC086iC07p06429, 1981.

Murto, S. and Tjernström, M.: Backward trajectories along the ship track using the LAGRANTO model, for the expedition ARTofMELT, Arctic Ocean, 2023, Bolin Centre Database., https://doi.org/https://doi.org/10.17043/oden-artofmelt-2023-trajectories- backward-ship-1, 2024.

https://doi.org/10.5194/egusphere-2026-1792
Preprint. Discussion started: 8 May 2026

Murto, S., Tjernström, M., Karalis, M., and Prytherch, J.: Wind, temperature, relative humidity, surface temperature and radiation from expedition ARTofMELT, Arctic Ocean, 2023. Dataset version 1, Bolin Centre Database., https://doi.org/10.17043/oden-artofmelt-2023-micromet-oden-1, 2024a.

Murto, S., Tjernström, M., Brooks, I., Guy, H., Karalis, M., Vihma, T., Urbancic, G., and Prytherch, J.: Radiosonde profiles from expedition ARTofMELT, Arctic Ocean, 2023, Bolin Centre Database., https://doi.org/https://doi.org/10.17043/oden-artofmelt-2023-radiosonde-1, 2024b.

Nilsson, E., Rannik, Ü., Swietlicki, E., Leck, C., Aalto, P. P., Zhou, J., and Norman, M.: Turbulent aerosol fluxes over the Arctic Ocean: 2. Wind-driven sources from the sea, Journal of Geophysical Research: Atmospheres, 106, https://doi.org/https://doi.org/10.1029/2000JD900747, 2001.

Nilsson, E. D. and Rannik, Ü.: Turbulent aerosol fluxes over the Arctic Ocean: 1. Dry deposition over sea and pack ice, Journal of Geophysical Research: Oceans, 106, https://doi.org/10.1029/2000JD900605, 2001.

Norris, S. J., Brooks, I. M., Leeuw, G., Sirevaag, A., Leck, C., Brooks, B. J., Birch, C. E., and Tjernstrom, M.: Measurements of bubble size spectra within leads in the Arctic summer pack ice, Ocean Science, https://doi.org/10.5194/osd-7-1739-2010, 2011.

Pereira Freitas, G., Adachi, K., Conen, F., Heslin-Rees, D., Krejci, R., Tobo, Y., Yttri, K. E., and Zieger, P.: Regionally sourced bioaerosols drive high-temperature ice nucleating particles in the Arctic, Nature Communications, 14, 5997, https://doi.org/10.1038/s41467-023-41696-7, 2023.

Pereira Freitas, G., Kojoj, J., Mavis, C., Creamean, J., Mattsson, F., Nilsson, L., Spicker Schmidt, J., Adachi, K., Šantl Temkiv, T., Ahlberg, E., Mohr, C., Riipinen, I., and Zieger, P.: A comprehensive characterisation of natural aerosol sources in the high Arctic during the onset of sea ice melt, Faraday Discussions, 258, 120–146, https://doi.org/10.1039/D4FD00162A, 2025.

Petelski, T. and Piskozub, J.: Vertical coarse aerosol fluxes in the atmospheric surface layer over the North Polar Waters of the Atlantic, Journal of Geophysical Research: Oceans, 111, https://doi.org/https://doi.org/10.1029/2005JC003295, 2006.

Prytherch, J., Yelland, M. J., Brooks, I. M., Tupman, D. J., Pascal, R. W., Moat, B. I., and Norris, S. J.: Motion-correlated flow distortion and wave-induced biases in air–sea flux measurements from ships, Atmospheric Chemistry and Physics, 15, 10 619–10 629, https://doi.org/https://doi.org/10.5194/acp-15-10619-2015, 2015.

Prytherch, J., Brooks, I. M., Crill, P. M., Thornton, B. F., Salisbury, D. J., Tjernström, M., Anderson, L. G., Geibel, M. C., and Humborg, C.: Direct determination of the air-sea CO2 gas transfer velocity in Arctic sea ice regions, Geophysical Research Letters, 44, 3770–3778, https://doi.org/10.1002/2017GL073593, 2017.

Ranjithkumar, A., Duncan, E., Yang, X., Partridge, D. G., Lachlan-Cope, T., Gong, X., Nishimura, K., and Frey, M. M.: Direct observation of Arctic Sea salt aerosol production from blowing snow and modeling over a changing sea ice environment, Elementa: Science of the Anthropocene, 13, https://doi.org/10.1525/elementa.2024.00006, 2025.

Rantanen, M., Karpechko, A. Y., Lipponen, A., Nordling, K., Hyvärinen, O., Ruosteenoja, K., Vihma, T., and Laaksonen, A.: The Arctic has warmed nearly four times faster than the globe since 1979, Communications Earth & Environment, 3, https://doi.org/10.1038/s43247-022-00498-3, 2022.

Saylor, R. D., Baker, B. D., Lee, P., Tong, D., Pan, L., and Hicks, B. B.: The particle dry deposition component of total deposition from air quality models: right, wrong or uncertain?, Tellus B: Chemical and Physical Meteorology, 71, https://doi.org/10.1080/16000889.2018.1550324, 2022.

Schmale, J., Zieger, P., and Ekman, A. M. L.: Aerosols in current and future Arctic climate, Nature Climate Change, 11, 95–105, https://doi.org/10.1038/s41558-020-00969-5, 2021.

https://doi.org/10.5194/egusphere-2026-1792
Preprint. Discussion started: 8 May 2026

Schmale, J., Sharma, S., Decesari, S., Pernov, J., Massling, A., Hansson, H.-C., von Salzen, K., Skov, H., Andrews, E., Quinn, P. K., Upchurch, L. M., Eleftheriadis, K., Traversi, R., Gilardoni, S., Mazzola, M., Laing, J., and Hopke, P.: Pan-Arctic seasonal cycles and long-term trends of aerosol properties from 10 observatories, Atmospheric Chemistry and Physics, 22, 3067–3096, https://doi.org/10.5194/acp-22-3067-2022, 2022.

Schneider, C. A., Rasband, W. S., and Eliceiri, K. W.: NIH Image to ImageJ: 25 years of image analysis, Nature Methods, 9, 671–675, https://doi.org/10.1038/nmeth.2089, 2012.

Scott, W. D. and Levin, Z.: Open channels in sea ice (leads) as ion sources, Science (New York, N.Y.), 177, 425–426, https://doi.org/10.1126/science.177.4047.425, 1972.

Serreze, M. C. and Barry, R. G.: Processes and impacts of Arctic amplification: A research synthesis, Global and Planetary Change, 77, 85–96, https://doi.org/10.1016/j.gloplacha.2011.03.004, 2011.

Shaw, G. E.: The Arctic Haze Phenomenon, Bulletin of the American Meteorological Society, 76, 2403–2414, https://doi.org/10.1175/1520-0477(1995)076<2403:TAHP>2.0.CO;2, 1995.

Song, C., Becagli, S., Beddows, D. C. S., Brean, J., Browse, J., Dai, Q., Dall'Osto, M., Ferracci, V., Harrison, R. M., Harris, N., Li, W., Jones, A. E., Kirchgäßner, A., Kramawijaya, A. G., Kurganskiy, A., Lupi, A., Mazzola, M., Severi, M., Traversi, R., and Shi, Z.: Understanding Sources and Drivers of Size-Resolved Aerosol in the High Arctic Islands of Svalbard Using a Receptor Model Coupled with Machine Learning, Environmental Science & Technology, 56, 11 189–11 198, https://doi.org/10.1021/acs.est.1c07796, 2022.

Sorbjan, Z. and Grachev, A. A.: An Evaluation of the Flux–Gradient Relationship in the Stable Boundary Layer, Boundary-Layer Meteorology, 135, 385–405, https://doi.org/10.1007/s10546-010-9482-3, 2010.

Spracklen, D. V., Carslaw, K. S., Kulmala, M., Kerminen, V., Sihto, S., Riipinen, I., Merikanto, J., Mann, G. W., Chipperfield, M. P., Wiedensohler, A., Birmili, W., and Lihavainen, H.: Contribution of particle formation to global cloud condensation nuclei concentrations, Geophysical Research Letters, 35, 2007GL033 038, https://doi.org/10.1029/2007GL033038, 2008.

Stevens, R. G., Loewe, K., Dearden, C., Dimitrelos, A., Possner, A., Eirund, G. K., Raatikainen, T., Hill, A. A., Shipway, B. J., Wilkinson, J., Romakkaniemi, S., Tonttila, J., Laaksonen, A., Korhonen, H., Connolly, P., Lohmann, U., Hoose, C., Ekman, A. M. L., Carslaw, K. S., and Field, P. R.: A model intercomparison of CCN-limited tenuous clouds in the high Arctic, Atmospheric Chemistry and Physics, 18, 11 041–11 071, https://doi.org/https://doi.org/10.5194/acp-18-11041-2018, 2018.

Swedish Polar Research Secretariat: ARTofMELT 2023, https://www.polar.se/en/expeditions/previous-expeditions/arctic/artofmelt-2023/, 2024.

Tan, I., Sotiropoulou, G., Taylor, P. C., Zamora, L., and Wendisch, M.: A Review of the Factors Influencing Arctic Mixed-Phase Clouds: Progress and Outlook, in: Clouds and Their Climatic Impacts, pp. 103–132, American Geophysical Union (AGU), ISBN 978-1-119-70035-7, https://doi.org/10.1002/9781119700357.ch5, 2023.

Tjernström, M. and Zieger, P.: Expedition report Atmospheric rivers and the onset of Arctic melt, ARTofMELT, 2023 with icebreaker Oden, Swedish Polar Research Secretariat, ISBN 978-91-519-5134-8, https://www.polar.se/en/expeditions/expedition-reports, 2025.

Tjernström, M., Birch, C. E., Brooks, I. M., Shupe, M. D., Persson, P. O. G., Sedlar, J., Mauritsen, T., Leck, C., Paatero, J., Szczodrak, M., and Wheeler, C. R.: Meteorological conditions in the central Arctic summer during the Arctic Summer Cloud Ocean Study (ASCOS), Atmospheric Chemistry and Physics, 12, 6863–6889, https://doi.org/10.5194/acp-12-6863-2012, 2012.

Tobo, Y., Adachi, K., Kawai, K., Matsui, H., Ohata, S., Oshima, N., Kondo, Y., Hermansen, O., Uchida, M., Inoue, J., and Koike, M.: Surface warming in Svalbard may have led to increases in highly active ice-nucleating particles, Communications Earth & Environment, 5, 516, https://doi.org/10.1038/s43247-024-01677-0, 2024.

https://doi.org/10.5194/egusphere-2026-1792
Preprint. Discussion started: 8 May 2026

Tunved, P., Ström, J., and Krejci, R.: Arctic aerosol life cycle: linking aerosol size distributions observed between 2000 and 2010 with air mass transport and precipitation at Zeppelin station, Ny-Ålesund, Svalbard, Atmospheric Chemistry and Physics, 13, 3643–3660, https://doi.org/10.5194/acp-13-3643-2013, 2013.

Twomey, S.: The Influence of Pollution on the Shortwave Albedo of Clouds, Journal of the Atmospheric Sciences, 34, 1149–1152, 1977.

Vickers, D. and Mahrt, L.: Quality Control and Flux Sampling Problems for Tower and Aircraft Data, Journal of Atmospheric and Oceanic Technology, 14, 512–526, https://doi.org/10.1175/1520-0426(1997)014<0512:QCAFSP>2.0.CO;2, 1997.

Wendisch, M., Macke, A., Ehrlich, A., Lüpkes, C., Mech, M., Chechin, D., Dethloff, K., Velasco, C. B., Bozem, H., Brückner, M., Clemen, H.-C., Crewell, S., Donth, T., Dupuy, R., Ebell, K., Egerer, U., Engelmann, R., Engler, C., Eppers, O., Gehrmann, M., Gong, X., Gottschalk, M., Gourbeyre, C., Griesche, H., Hartmann, J., Hartmann, M., Heinold, B., Herber, A., Herrmann, H., Heygster, G., Hoor, P., Jafariserajehlou, S., Jäkel, E., Järvinen, E., Jourdan, O., Kästner, U., Kecorius, S., Knudsen, E. M., Köllner, F., Kretzschmar, J., Lelli, L., Leroy, D., Maturilli, M., Mei, L., Mertes, S., Mioche, G., Neuber, R., Nicolaus, M., Nomokonova, T., Notholt, J., Palm, M., van Pinxteren, M., Quaas, J., Richter, P., Ruiz-Donoso, E., Schäfer, M., Schmieder, K., Schnaiter, M., Schneider, J., Schwarzenböck, A., Seifert, P., Shupe, M. D., Siebert, H., Spreen, G., Stapf, J., Stratmann, F., Vogl, T., Welti, A., Wex, H., Wiedensohler, A., Zanatta, M., and Zeppenfeld, S.: The Arctic Cloud Puzzle: Using ACLOUD/PASCAL Multiplatform Observations to Unravel the Role of Clouds and Aerosol Particles in Arctic Amplification, Bulletin of the American Meteorological Society, 100, 841–871, https://doi.org/10.1175/BAMS-D-18-0072.1, 2019.

Westergaard-Nielsen, A., Karami, M., Hansen, B. U., Westermann, S., and Elberling, B.: Contrasting temperature trends across the ice-free part of Greenland, Scientific Reports, 8, https://doi.org/10.1038/s41598-018-19992-w, 2018.

Whaley, C. H., Mahmood, R., von Salzen, K., Winter, B., Eckhardt, S., Arnold, S., Beagley, S., Becagli, S., Chien, R.-Y., Christensen, J., Damani, S. M., Dong, X., Eleftheriadis, K., Evangeliou, N., Faluvegi, G., Flanner, M., Fu, J. S., Gauss, M., Giardi, F., Gong, W., Hjorth, J. L., Huang, L., Im, U., Kanaya, Y., Krishnan, S., Klimont, Z., Kühn, T., Langner, J., Law, K. S., Marelle, L., Massling, A., Olivié, D., Onishi, T., Oshima, N., Peng, Y., Plummer, D. A., Popovicheva, O., Pozzoli, L., Raut, J.-C., Sand, M., Saunders, L. N., Schmale, J., Sharma, S., Skeie, R. B., Skov, H., Taketani, F., Thomas, M. A., Traversi, R., Tsigaridis, K., Tsyro, S., Turnock, S., Vitale, V., Walker, K. A., Wang, M., Watson-Parris, D., and Weiss-Gibbons, T.: Model evaluation of short-lived climate forcers for the Arctic Monitoring and Assessment Programme: a multi-species, multi-model study, Atmospheric Chemistry and Physics, 22, 5775–5828, https://doi.org/10.5194/acp-22-5775-2022, 2022.

Wilczak, J. M., Oncley, S. P., and Stage, S. A.: Sonic Anemometer Tilt Correction Algorithms, Boundary-Layer Meteorology, 99, 127–150, https://doi.org/10.1023/A:1018966204465, 2001.

Willis, M. D., Leaitch, W. R., and Abbatt, J. P.: Processes Controlling the Composition and Abundance of Arctic Aerosol, Reviews of Geophysics, 56, 621–671, https://doi.org/10.1029/2018RG000602, 2018.

Yang, X., Frey, M. M., Rhodes, R. H., Norris, S. J., Brooks, I. M., Anderson, P. S., Nishimura, K., Jones, A. E., and Wolff, E. W.: Sea salt aerosol production via sublimating wind-blown saline snow particles over sea ice: parameterizations and relevant microphysical mechanisms, Atmospheric Chemistry and Physics, 19, 8407–8424, https://doi.org/10.5194/acp-19-8407-2019, 2019.

You, Q., Cai, Z., Pepin, N., Chen, D., Ahrens, B., Jiang, Z., Wu, F., Kang, S., Zhang, R., Wu, T., Wang, P., Li, M., Zuo, Z., Gao, Y., Zhai, P., and Zhang, Y.: Warming amplification over the Arctic Pole and Third Pole: Trends, mechanisms and consequences, Earth-Science Reviews, 217, https://doi.org/10.1016/j.earscirev.2021.103625, 2021.

Zhang, L., Gong, S., Padro, J., and Barrie, L.: A size-segregated particle dry deposition scheme for an atmospheric aerosol module, Atmospheric Environment, 35, 549–560, https://doi.org/10.1016/S1352-2310(00)00326-5, 2001.